Dalton Transactions

An international journal of inorganic chemistry

Accepted Manuscript

This article can be cited before page numbers have been issued, to do this please use: P. Ghorai, K. Pal, P. Karmakar and A. Saha, *Dalton Trans.*, 2020, DOI: 10.1039/C9DT04902A.

ROYAL SOCIETY OF CHEMISTRY

rsc.li/dalton

View Article Online
DOI: 10.1039/C9DT04902A

Development of two fluorescent chemosensors for selective detection of Zn^{2+} and Al^{3+} ions in quinoline platform by tuning of substituent in the receptor part: Elucidation of structures of metal bound chemosensors and biological studies

Pravat Ghorai,[a] Kunal Pal,[b] Parimal Karmakar,[b] and Amrita Saha*[a]

[a]*Department of Chemistry, Jadavpur University, Kolkata- 700032, India.*

E-mail: amritasahachemju@gmail.com; Tel. +91-33-24572146

[b]*Department of Life Science and Biotechnology, Jadavpur University, Kolkata-700032, India.*

Abstract

Here, 8-aminoquinoline based two chemosensors $\mathbf{HL_1}$ and $\mathbf{HL_2}$ ($\mathbf{HL_1}$ = 2,4-Dibromo-6-((quinolin-8-ylimino)methyl)phenol and $\mathbf{HL_2}$ = 4-Nitro-2-((quinolin-8-ylimino)methyl)phenol) have been achieved by simply changing substituents in the ligand framework under ambient condition. They are thoroughly characterized by different spectroscopic techniques, ESI-mass and elemental analysis. $\mathbf{HL_1}$ selectively sense Zn^{2+} ion whereas, $\mathbf{HL_2}$ detect Al^{3+} ion. The investigation of metal bound chemosensors (complexes **1** and **2**) are also done by different techniques including X-ray crystallography. 2:1 binding stoichiometry of the probes with the respective ions has been confirmed by Job's plot analysis and X-ray crystallography. The limit of detection (LOD) values for both the chemosensors towards the respective metal ions are in $\sim 10^{-7}$ M order which clearly indicate that the probes have significant potential for biological application. The capability of our synthesized chemosensors to detect intracellular Zn^{2+} and Al^{3+} ions in triple negative human breast cancer cell line *MDA-MB-468* is evaluated with the aid of fluorescence imaging. The mechanistic insight into the anticancer activity of complexes **1** and **2** are also demonstrated in this study. To the best of our knowledge, we are the first time to

View Article Online
DOI: 10.1039/C9DT04902A

envisage such type of biological and sensing activity of 8-aminoquinoline based complexes in a single platform.

Introduction

Selective detection of target molecules/species could be achieved by judicial choice of various receptors, equipped with certain responsive groups which are capable of exhibiting optical,[1] magnetic or electrochemical signals. Among different sensing techniques, fluorescence sensing process[2] is one of the most frequently used technique due to its user friendly operation procedure and simple instrumentation.[3] This process also has quick response time, high selectivity and sensitivity towards analyte molecules.[4-7] Target molecules/species could be cationic, anionic or neutral species, among them Zn^{2+} and Al^{3+} need special mention. In biological systems Zn^{2+} is the second most abundant transition metal after iron.[8] The concentration of Zn^{2+} in human body varies differently. In intracellular serum Zn^{2+} is present in 12 μM level whereas, in brain and nerve tissues its abundance is 0.1-0.5 μM.[9,10] Zn^{2+} is found in proteins and peptides in tightly bound form. Whereas, in brain,[11] pancreas,[12] spermatozoa,[13] paneth cells in the intestine, mast cells, granulocytes, pituitary cells and CNS neurons,[14] Zn^{2+} is present as free or chelatable form. In the brain, Zn^{2+} is sequestered in the vesicles of presynaptic neurons and it releases Zn^{2+} in active form. Zn^{2+} is found to induce the formation of *β*-amyloid (*β*A),[15] which is related to the etiology of Alzheimer's disease.[16,17] In amyloid plaques concentration of Zn^{2+} is high, 0.2-1 mM. Pancreatic *β*-cells simultaneously release chelatable Zn^{2+} and insulin and local concentration of Zn^{2+} surrounding activated *β*-cells is found as 0.48 mM.[18] Therefore, monitoring release of Zn^{2+} from *β*-cells *in vivo* will help to understand the etiology and treatment of diabetes.[19] Zn^{2+} is a d^{10} system and it has very similar electronic properties to that of Cd^{2+} ions. Therefore, development of fluorescent chemosensors for the

View Article Online
DOI: 10.1039/C9DT04902A

selective and sensitive detection of zinc ions especially in the field of biological environment is a challenging task.[20] Al^{3+} ions have huge impact in human society due to multi-dimensional role and diverse applications of Al-containing compounds. Catalytic activity β-AlF_3 compound initiates conversion of ozone-depleting reagent CFCs into environmentally acceptable HFCs.[21] Aluminum MOFs (Al-MOFs) could be used in different fields such as, sorption, separations, purification of water and air, heterogeneous catalysis, sensing.[22] According to European Food Safety Agency (EFSA) tolerable weekly intake of aluminium is 1 mg Al/kg of body weight per week.[23] In 1976, first time, aluminium toxicity was noticed in haemodialysis patients. In 1978, first time,[24] osteomalacia or "aluminium-induced bone disease" (AIBD), due to aluminium overload was observed.[25] Acid rain is responsible for release of aluminium from mineral deposits, which is finally appears as pollutant in waters.[26] Aluminium is highly available in coffee and tea plants, which are cultivated on acid soil. Such plants are responsible for dietary aluminium exposure to humans.[27,28] In the aluminium industry, workers suffer from[29] bladder, leukemia, lung, renal, pancreatic and brain cancer[30] due to higher aluminium exposure. Aluminium intoxication inhibits activity of superoxide dismutase (SOD) and catalase, thus modify both glial and neuronal nitric oxide synthesis, and enhance DNA fragmentation.[31-33] Aluminium accumulation in the brain causes neuron degeneration followed by different diseases such as Parkinson's disease, Alzheimer's disease, dialysis encephalopathy, amyotrophic lateral sclerosis, and multiple sclerosis.[34-37]

Among different Al^{3+} ion detection techniques like inductively coupled plasma atomic emission spectroscopy and graphite furnace atomic absorption spectrometry techniques are most frequently used for real sample analysis. Preparation of fluorescent chemosensor for selective detection of Al^{3+} ion is a challenging task due to its weak coordination ability and strong

View Article Online
DOI: 10.1039/C9DT04902A

hydration ability. Most of the time trivalent ions like Cr^{3+} and Fe^{3+} interfere in Al^{3+} ion detection. Common fluorophoric units present in Al^{3+} ion sensing chemosensors are rhodamine, anthraquinone, BODIPY, salicylaldehyde, fluorescein, coumarin, etc.[38-44] Whereas, common Zn^{2+} sensing chemosensors are di-2-picolylamine (DPA),[45-48] quinoline,[49-55] bipyridyl[56] etc. Important fluorescence sensing mechanisms are photo induced electron transfer (PET), fluorescence resonance energy transfer (FRET), intermolecular charge transfer (ICT) and chelation induced enhanced fluorescence (CHEF) mechanisms.[56,57-60]

Some recently reported quinoline based chemosensors are collected in Chart S1[55] (Supporting Information). Chart S1 clearly indicates that chemosensors reported in this work have certain advantages in different areas such as crystal structure elucidation of metal bound chemosensors, excitation wavelength in visible region, cell imaging studies of chemosensors and study of anticancer activities of the isolated chemosensor bound metal complexes in comparison with previously reported data. K. Xu *et al*. have reported a quinoline based dual-chemosensor,[55a] which act as a fluorescent-colorimetric probe for selective detection of both Zn^{2+} and Al^{3+} ions. Furthermore, chemosensor bound Al^{3+} system is used for fluoride ion detection. The sensitivity of the probe (limit of detection, LOD value) towards metal (Zn^{2+} and Al^{3+}) ions fall in the nano molar range (11.5 nM and 23.5 nM, respectively). P. Roy and his group[55b] have reported two aminoquinoline based dual-chemosensors which selectively sense Al^{3+} and Zn^{2+} ions. X. Chen *et al.*[55g] have developed a simple ratiomatric fluorescent chemosensor for selective detection of Zn^{2+} ions and secondary detection for $H_2PO_4^-$ ion. The LOD value of the chemosensor towards Zn^{2+} ions is found in nanomolar range (41.0 nM). D. Bai and his group[55l] have synthesized a fluorescent probe for selective detection of Zn^{2+} ions. The chemosensor is capable of discriminating Zn^{2+} from Cd^{2+} in living cells and plant tissues. In above works, neither crystal

View Article Online
DOI: 10.1039/C9DT04902A

structure of free chemosensors nor their metal bound complexes are reported. R. Fan *et al.*[55f] have described a quinoline based fluorescent dual-chemosensor which selectively detect $Zn^{2+}$and Hg^{2+} ions based on CHEF mechanism. Interestingly, they have reported crystal structures of both metal bound chemosensor complexes. The LOD value of the chemosensor towards Zn^{2+} ion is 0.011 μM. M. Amirnasr and his coworkers[55h] have reported a chemosensor on quinoline platform for fluorometric detection of Zn^{2+} ions and colorimetric detection of Cu^{2+} ions. Another interesting aminoquinoline based chemosensing work have been reported by P. Roy and his group for selective detection of Al^{3+} ion and secondary detection for F^{-} ions.[55i] Here the LOD value for Al^{3+} ion is observed in very low range (75.19 nM). Chemosensor reported by Y.-M. Zhang *et al.*[55j] is used for both colorimetric detection for F^{-} and a fluorescence detection of Zn^{2+}. Here Zn^{2+} detection is based on excited-state intramolecular proton transfer (ESIPT) mechanism. Y. Yue *et al*.[55m] have reported a "turn-on" fluorescent probe for detection of Zn^{2+} ions in $CH_3OH–H_2O$ solution. The chemosensor is further used to detect Zn^{2+} in river water. In above examples live cell imaging studies of the chemosensors are not performed. S. Mukherjee and her group[55k] have reported a chemosensor for selective detection of Zn^{2+} ion in aqueous methanol medium. They have also established molecular 'INHIBIT' logic gate with $Zn^{2+}$and EDTA as chemical inputs. The chemosensor is further used for sensing Zn^{2+} in real sample analysis. C. Kim and coworkers[55n] have synthesized a water-soluble fluorescent 'turn-on' chemosensor for zinc ions in aqueous buffer solution. The calculated LOD value for Zn^{2+} ions is very low, 4.48 μM. The sensor is also used to detect Zn^{2+} in real water samples. S. Erdemir and his group[55q] are reported a duel-chemosensor for detection of Zn^{2+}, Al^{3+} cations in EtOH-H_2O and F^{-} anion in acetonitrile medium. In the above research works neither crystal structure of the chemosensor nor live cell imaging studies are reported. In another interesting work of M. Amirnasr *et al*.,[55c] a

View Article Online
DOI: 10.1039/C9DT04902A

chemosensor is reported which show turn on fluorescence in presence of Zn^{2+} ion and colorimetric changes in presence of Co^{2+} ion in acetonitrile medium. They have successfully elucidated the metal bound X-ray crystal structure. The excitation wavelength for detection of Zn^{2+} ion is 370nm. A water soluble Zn^{2+} ion sensing probe has been developed by Z. Wang and coworkers.[55d] The chemosensor is excited at 350nm during fluorometric detection of metal ions. M. Sukwattanasinitt and his group[55e] have synthesized two amide derivatives based on 8-aminoquinoline and amino acids, glycine and β-alanine respectively for selective detection of Zn^{2+} and Cd^{2+} ions. The limit of detection of chemosensing probe, towards Zn^{2+} ion is in micromolar range (1.6 μM). The excitation wavelength for detection of Zn^{2+} ion is 300 nm. In the above examples chemosensors are excited in UV-region. Excitation wavelength at UV-region disfavor real sample and biological sample analysis.

In this work, we have designed two quinoline based chemosensors (**HL_1** and **HL_2**) for selective detection of Zn^{2+} and Al^{3+} ions. Main disadvantage of quinoline based chemosensors is the presence of fluorescence excitation wavelength in the UV-region. In this sensing experiment, fluorescence excitation wavelengths of both the chemosensors appear in the visible region. Visible range excitation wavelengths make these systems promising probe in the field of biological study. Interesting aspect of this work is achievement of both chemosensors by simply changing substituent in the ligand framework. Substituent change in the receptor part (metal ion binding sites) of the ligand framework is based on HSAB theory. Due to hard basic character of the nitro-substituted chemosensor, it selectively detects Al^{3+} ions. On the contrary, bromo substituted chemosensor selectively detects Zn^{2+} ions due to its comparatively soft rather intermediate basic character. Chemosensors **HL_1** and **HL_2** result 30 times and 29 times enhancement of emission intensity in presence of Zn^{2+} and Al^{3+} ions, respectively. The detection

View Article Online
DOI: 10.1039/C9DT04902A

limit (LOD) of $\mathbf{HL_1}$ and $\mathbf{HL_2}$ against Zn^{2+} and Al^{3+} ions are 1.39×10^{-7} M and 1.50×10^{-7} M, respectively which clearly indicate that the probes can be used to detect Zn^{2+} and Al^{3+} ions in biological system. Binding affinity of both metal ions towards the chemosensors $(1.33\pm0.04) \times 10^4$ M^{-1} and $(1.65\pm0.008) \times 10^4$ M^{-1}, for complexes **1** and **2**, respectively) and the values of quantum yield of metal bound chemosensors (0.17 and 0.21 for complexes **1** and **2**, respectively) suggest that the probes have significant affinity towards the respective metal ions. We are successfully elucidated X-ray crystal structure of both Al^{3+} and Zn^{2+} ions bound chemosensor complexes. X-ray crystal structures also confirm fluorescence enhancing mechanism as PET Off-CHEF On process. To best of our knowledge, crystal structure of Al^{3+} bound quinoline based chemosensor complexes are scarce in literature. Furthermore, these biocompatible chemosensors also exhibit cell permeability and sense intracellular ions in breast cancer cell line, *MDA-MB-468* cells. Both the complexes **1** and **2** show considerable cytotoxicity toward *MDA-MB 468* and *SiHa* cells. Our observations suggest that the induction of apoptosis occurs after treatment with complex **1** and complex **2** which ultimately culminates in the cell death. Therefore, we can conclude that these complexes exhibit promising anticancer activities.

Results and discussion

Synthesis and characterization

Derivatives of 8-aminoquinoline are used as chelating ligands for preparation of interesting luminescent metal–organic materials. The luminescent properties of these complexes mainly dependent on nature of metal ions and coordination of the metal ions with the ligand scaffold. 8-hydroxyquinoline upon reaction with different aldehydes generates Schiff base ligands which can be easily stabilized in presence of metal ion. The photophysical behavior of

View Article Online
DOI: 10.1039/C9DT04902A

these complexes can be tunable by modification on either the 8-aminoquinoline part or the aldehyde part.

Here, quinoline based two Schiff base ligands (**HL_1** and **HL_2**) are prepared by following a usual procedure.[61] 3,5-dibromosalicyladehde and 2-hydroxy-5-nitrobenzaldehyde upon reaction with 8-aminoquinoline in 1:1 molar ratio in methanolic solution under ambient condition (Scheme S1, Supporting Information) generate Schiff base ligands **HL_1** and **HL_2**, respectively. The chemosensors (**HL_1** and **HL_2**) are obtained in solid form with high yield. Characterization and purity are established using different spectroscopic methods (UV-Vis, FT-IR and ^{1}H, ^{13}C NMR) and elemental analysis. In the ESI-MS spectrum of the chemosensors, the base peak is appeared at *m/z* = 406.98 and 294.11, corresponding to $[\mathbf{HL_1}+H]^+$ and $[\mathbf{HL_2}+H]^+$, respectively (Fig. S1 and S2, Supporting Information). In the FT-IR spectrum of **HL_1** and **HL_2**, a band appear at around 1605 cm^{-1} is attributed as C=N (for azomethine) stretching frequency (Fig. S3 and S4, Supporting Information).

HL_1 reacts with $Zn(NO_3)_2.6H_2O$ in 2:1 molar ratio to produce complex **1.** Similarly, **HL_2** reacts with $Al(NO_3)_3.9H_2O$ in 2:1 molar ratio to produce complex **2** (Scheme 1). Both the complexes crystallize from chloroform-methanol (v/v, 1:1) solvent mixture. They are characterized by X-ray crystallography, elemental and ESI-MS analyses. Experimentally observe *m/z* values 923.52 and 611.29 corresponding to molecular ion peak of $[Zn(\mathbf{L_1})_2+CH_3CN+Li]^+$ and $[Al(\mathbf{L_2})_2]^+$, respectively (Fig. S5 and S6, Supporting Information). Experimental observations are well matched with the simulated pattern. In FT-IR spectrum of complex **1**, the characteristics stretching frequencies appear at 1615 cm^{-1} for (C=N) and 759 cm^{-1} for (C-H) bonds. Similarly, in case of complex **2** characteristics stretching frequencies appear at 1615cm^{-1} [υ(C=N)], 1318 cm^{-1} [(υ(NO_3^-), asymmetric stretch] and 771 cm^{-1} [υ(C-H)], respectively (Fig. S7

View Article Online
DOI: 10.1039/C9DT04902A

and S8, Supporting Information). Thermal stability of the chemosensors (**HL_1** and **HL_2**) and the metal complexes (**1** and **2**) has been checked by TGA (Thermo Gravimetric Analysis). Both chemosensors are stable up to 250°C whereas complexes **1** and **2** are stable up to 350°C (Fig. S9, Supporting Information).

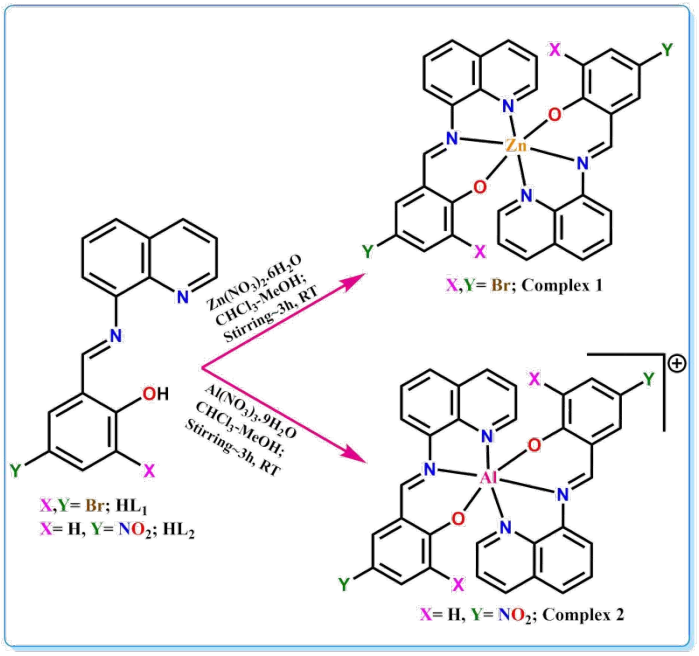

Scheme 1 Route of synthesis of complexes **1** and **2**.

Crystal structure description of complexes 1 and 2

Both complexes **1** and **2** are mononuclear. Complex **1**, $\{[Zn(\mathbf{L_1})_2].CHCl_3\}$ crystallizes in triclinic form with *P-1* space group, whereas, complex **2**, $\{[Al(\mathbf{L_2})_2](NO_3)\}$ crystallizes in monoclinic form with *P* $2_1/n$ space group (Table S1, Supporting Information). The crystal structural of complexes **1** and **2** are shown in Fig. 1 and 2, respectively. Selected bond distances and angles are collected in Table 1. The crystal structure of complex **1** contains one chloroform unit as a solvent molecule whereas, in complex **2** nitrate ion is present as counter ion. Both complexes are distorted octahedral where, two deprotonated ligands ($\mathbf{L_1}^{-1}$ or $\mathbf{L_2}^{-1}$) bind the metal ion (Zn^{2+} or Al^{3+}) in a N_2O fashion involving a phenoxido oxygen atom (O1, O2), imine nitrogen

View Article Online
DOI: 10.1039/C9DT04902A

atom (N2, N4) and quinoline nitrogen atom (N1, N3). In the octahedral structures each of the coordinating sites occupies one meridional position around the metal centers. The four chelate bite angles in complex **1** (N3–Zn–N4, N4–Zn–O2, N1–Zn–N2 and N2–Zn–O1) vary within range 75.8(3)°–88.3(3)°. In complex **2**, chelate bite angles (N3–Al–N4, N4–Al–O2, N1–Al–N2 and N2–Al–O1) vary within range 80.91(10)°–91.97(10)°. Zn–N(quinoline) bond distances are relatively longer compared to Zn–O (phenoxido) bond distances. Similarly, Al–N (quinoline) bond distances are relatively longer than Al–O (phenoxido) bond distances. The solid state structure of **1** is stabilized by edge-to-edge π···π stacking along the ab plane with the distances 3.484 Å and 3.512 Å, respectively and nonconventional halogen···π, halogen···halogen interactions along a axis with shortest distances 3.525 Å and 3.639 Å, respectively (Fig. S10a and S10b, Supporting Information). In case of **2,** a similar π···π stacking and nonconventional C–H···π interactions has been found along the c axis with shortest distances 3.569 Å and 2.909 Å, respectively (Fig. S11, Supporting Information).

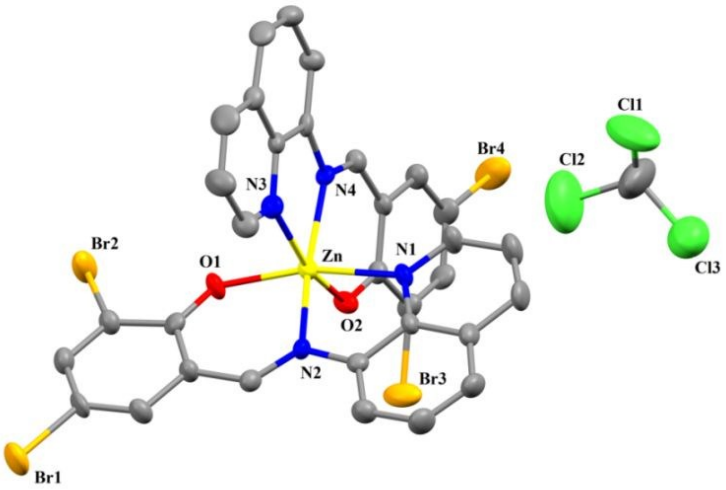

Fig. 1 Crystal structure of complex **1**. Atoms are shown as 30% thermal ellipsoids. H atoms are omitted for clarity.

View Article Online
DOI: 10.1039/C9DT04902A

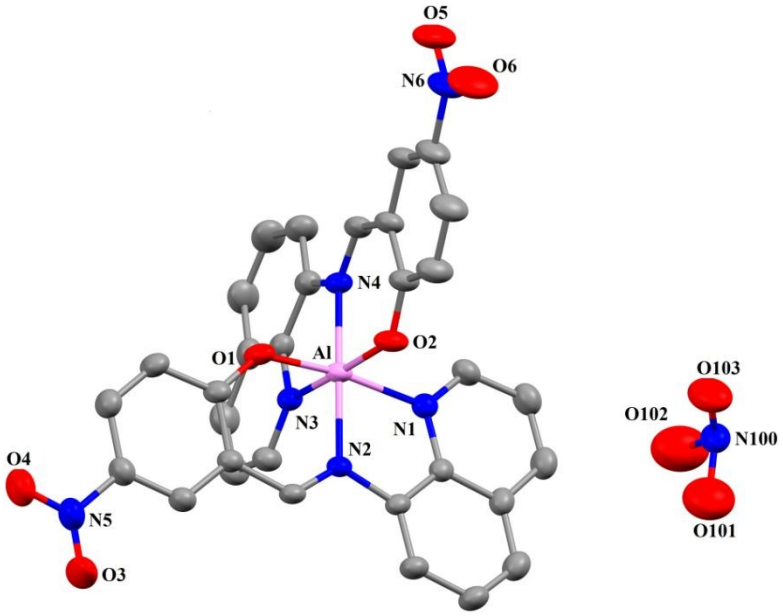

Fig. 2 Crystal structure of complex **2**. Atoms are shown as 30% thermal ellipsoids. H atoms are omitted for clarity.

Table 1 Selected bond lengths (Å) and bond angles (°) for complexes **1** and **2**

Complex **1**				Complex **2**			
Zn-O1	2.055(7)	Zn-N4	2.121(8)	Al-O1	1.815(2)	Al-N4	1.993(2)
Zn-O2	2.047(7)	O1-Zn-N2	88.3(3)	Al-O2	1.823(2)	O1-Al-N2	91.97(10)
Zn-N1	2.212(8)	O2-Zn-N4	88.1(3)	Al-N1	2.039(3)	O2-Al-N4	91.73(10)
Zn-N2	2.126(8)	N1-Zn-N2	76.3(3)	Al-N2	1.990(2)	N1-Al-N2	80.91(10)
Zn-N3	2.218(8)	N4-Zn-N3	75.8(3)	Al-N3	2.044(3)	N4-Al-N3	81.44(10)

View Article Online
DOI: 10.1039/C9DT04902A

NMR studies

^{1}H NMR spectral studies of chemosensors (**HL_1** and **HL_2**) have been performed in DMSO-d_6 solvent (Fig. S12 and S13, Supporting Information). In case of **HL_1**, phenolic -OH and imine (H-C=N) proton appear as singlet at 15.94 ppm and 9.27 ppm, respectively. The eight aromatic protons appear in the range 7.69–9.06 ppm, whereas, for **HL_2**, aromatic protons appear in the range 6.90–9.05 ppm. In **HL_2** a broad peak has been found at 16.03 ppm which can be assigned as phenolic –OH group and a sharp peak at 9.53 ppm can be assigned as imine (H-C=N) proton. ^{1}H NMR titration experiment has been performed between chemosensors (**HL_1** and **HL_2**) and respective metal ions (Zn^{2+} and Al^{3+}) in DMSO-d_6 solvent in order to establish their coordination mechanism. In both experiments metal ions are added gradually in 0.125 equivalents to one equivalent of ligand solution. 0.125 equivalents addition of Zn^{2+} ions in **HL_1**, signal for phenolic OH proton become broaden and finally disappears upon 0.5 equivalents addition of Zn^{2+} ions. It clearly indicates metal coordination with phenoxido oxygen atom. (Fig. S14(a), Supporting Information) Again, imine proton (H-C=N) gradually shifted towards downfield from 9.269 ppm to 9.321 ppm (after adding 0.50 equivalent Zn^{2+} ions to the **HL_1**), suggesting Zn^{2+} coordination with imine nitrogen atom. Zn^{2+} coordination with imine and quinoline nitrogen atoms of **HL_1** also results broadening and splitting of both phenyl and quinoline ring protons. Thus all the data confirm complexation between Zn^{2+} and **HL_1**. Similar result has been noticed in case of Al^{3+} ions. Where, gradual addition of Al^{3+} ions in **HL_2** result disappearances of phenolic OH proton, shifting of imine (H-C=N) proton (from 9.52 ppm to 10.10 ppm) and broadening and splitting of both phenyl and quinoline ring protons. Interestingly, broadening and shifting of these protons are more prominent in case of Al^{3+} ions (Fig. S14(b), Supporting Information). This result again confirms complexation between Al^{3+} and **HL_2**.

View Article Online
DOI: 10.1039/C9DT04902A

Importantly, proton titration data are match well with the individual ^{1}H NMR data of complexes **1** and **2**. In complex **1**, phenolic OH protons are absent, imine protons appear at downfield, 9.34 ppm and aromatic protons appear in the range 7.43–8.48 ppm. Similarly, for complex **2**, phenolic OH protons are absent, imine protons appear at downfield, 10.27 ppm and aromatic protons have been found in the range 6.61–8.96 ppm (Fig. S15 and S16, Supporting Information).

^{13}C NMR spectra of $\mathbf{HL_1}$ and $\mathbf{HL_2}$ are also examined in DMSO-d_6 solvent (Fig. S17 and S18, Supporting Information). The imine carbon atom of $\mathbf{HL_1}$ appears at 163.83 ppm whereas aromatic carbon atoms appear in the range 106.84–160.72 ppm. Similarly, for $\mathbf{HL_2}$, imine carbon atom appears at 161.62 ppm and aromatic carbon atoms appear in the range 117.94–151.49 ppm. In ^{13}C NMR spectra of complexes **1** and **2**, imine carbon atoms appear at 163.71 and 170.41 ppm, respectively. Rest of the carbon atoms has been found within the range 111.70–156.40 ppm and 118.40–167.96 ppm respectively (Fig. S19 and S20, Supporting Information).

Absorption spectral studies

The UV-Vis spectra of the chemosensors ($\mathbf{HL_1}$ and $\mathbf{HL_2}$) are examined in 10 mM HEPES buffer at pH 7.4. Characteristic bands around 480 nm and 340 nm for $\mathbf{HL_1}$ and 450 nm and 325 nm for $\mathbf{HL_2}$ suggest n→π* and π →π* type of transitions within the probes. Gradual addition of Zn^{2+} ions to a 10 μM $\mathbf{HL_1}$ solution result disappearance of the peak at 480 nm and concomitant appearance of a new band at around 440 nm (Fig. 3). Significant hypsochromic shift (~ 40 nm) of the original peak at 480 nm confirms coordination of the Zn^{2+} ions with the probe. Saturation of the peak after addition of 5 μM Zn^{2+} ions suggests 2:1 binding between probe and Zn^{2+} ions. Similarly, in presence of Al^{3+} ions, large hypsochromic shift (~ 50 nm) of the original peak of free chemosensor $\mathbf{HL_2}$ (10 μM) from 450 nm to 398 nm confirm coordination of Al^{3+} ions with

View Article Online
DOI: 10.1039/C9DT04902A

the probe. Again, saturation of the peak after addition of 5 μM Al^{3+} ions indicates 2:1 binding between probe and Al^{3+} ions (Fig. 4).

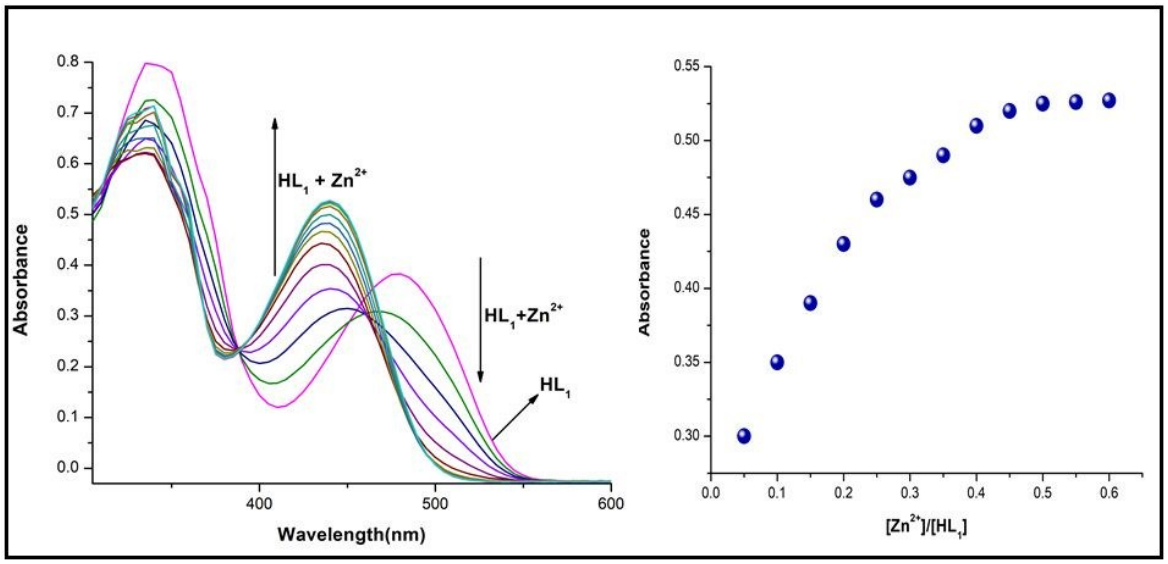

Fig. 3 UV-Vis. titration of $\mathbf{HL_1}$ (10 μM) with gradual addition of Zn^{2+}ions (0-6 μM) in 10 mM HEPES buffer at pH 7.4 and corresponding absorbance versus molar ratio plot.

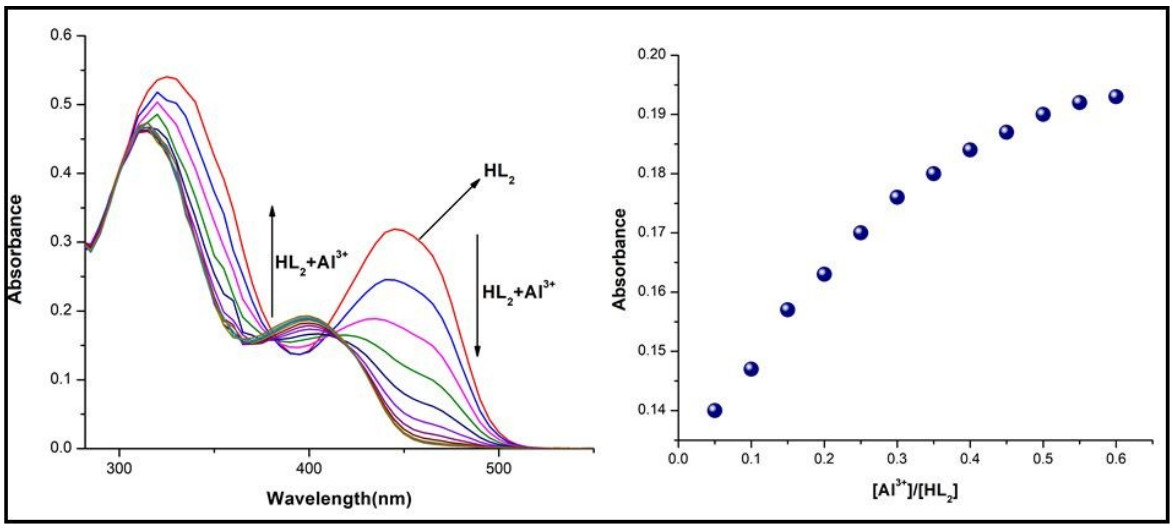

Fig. 4 UV-Vis. titration of $\mathbf{HL_2}$ (10 μM) with gradual addition of Al^{3+} ions (0-6 μM) in 10 mM HEPES buffer at pH 7.4 and corresponding absorbance versus molar ratio plot.

View Article Online
DOI: 10.1039/C9DT04902A

Job's plot analysis confirms 2:1binding stoichiometry of probes with the respective ions (Fig. S21 and S22, Supporting Information). Interestingly, X-ray crystallography and ESI-mass analysis also support 2:1 binding stoichiometry. Binding constant values for Zn^{2+} and Al^{3+} ions towards **HL_1** and **HL_2** are calculated using non-linear least-square curve fit equation (equation 1).[55o]

$$y = \left(\frac{a + b \times x\hat{}n}{1 + c \times x\hat{}n}\right) \quad \ldots\ldots\ldots\ldots\ldots\ldots\ldots\ldots (1)$$

Where, 'a' and 'b' are the absorbance or emission in absence and presence of excess metal ions, respectively. 'c' is formation constant or binding constant (k) whereas '*n'* is binding stoichiometry of the reaction. The estimated value of '*n'* is closely to the 0.5 and calculated binding constant values are (1.33±0.04) × 10^4 M^{-1} and (1.65±0.008) × 10^4 M^{-1}, respectively (Fig. S23 and S24, Table S2, Supporting Information) for Zn^{2+}-**HL_1** and Al^{3+}-**HL_2** adduct.

Fluorescence properties

All the fluorescence experiments are performed in 10 mM HEPES buffer (pH = 7.4) at ambient conditions. Upon excitation at 480 nm and 450 nm, **HL_1** and **HL_2** exhibit weak fluorescence at around 545 and 515 nm, respectively. This is probably due to PET (Photoinduced Electron Transfer) process. Gradual addition of Zn^{2+} ions (6 μM) to **HL_1** (10 μM), results great enhancement of emission intensity (30 times, excitation wavelength 440 nm) with slight (5 nm) blue shift of the emission peak (Fig. 5). Saturation of the peak has been observed after 0.5 equivalents addition of Zn^{2+} ions. Coordination of phenoxido-O, imine-N and quinoline-N atoms of the probe with Zn^{2+} results increase of rigidity the ligand system (CHEF effect) via inhibition of free rotation around the H–C=N bond. Involvement of lone pairs of imine nitrogen also hinders PET process. These two effects are jointly responsible for the fluorescence enhancement.

View Article Online
DOI: 10.1039/C9DT04902A

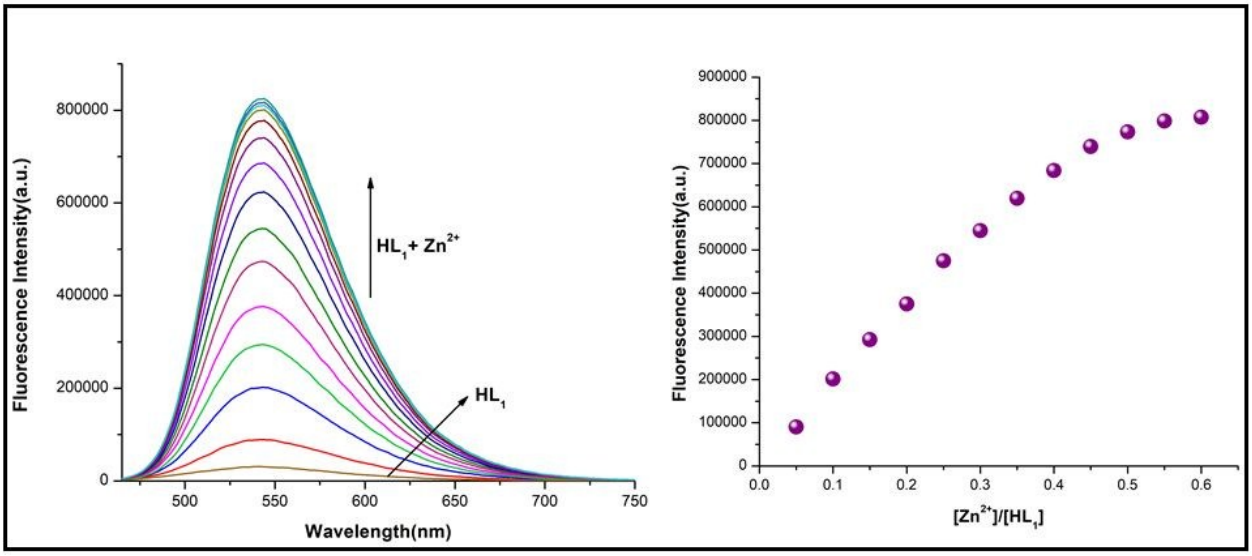

Fig. 5 Fluorescence titration of $\mathbf{HL_1}$ (10 μM) with gradual addition of Zn^{2+} (0-6 μM) in 10 mM HEPES buffer at pH 7.4 and corresponding fluorescence intensities versus molar ratio plot.

Al^{3+} ions sensing experiment is performed in presence of chemosensor $\mathbf{HL_2}$, where, enhancement (~29 fold) of fluorescence emission at ~475 nm (excitation wavelength 400 nm) is observed (Fig. 6). Interestingly, hypsochromic shift is large (around 40 nm). Here, coordination of phenoxido-O, imine-N and quinoline-N atoms of the probe with Al^{3+} results increase of rigidity the ligand system (CHEF effect). Enhancement in the fluorescence intensity for both the ions can be explained by PET-OFF, CHEF-ON process. This type of mechanistic pathway has been further verified by X-ray crystallography.

Both chemosensors are achieved based on judicial selection of substituent in the ligand framework. Chemo selectivity of the Zn^{2+} and Al^{3+} ions by $\mathbf{HL_1}$ and $\mathbf{HL_2}$ is based on HSAB theory. Nitro-substitution makes $\mathbf{HL_2}$ a hard base which selectively detects Al^{3+} ions. Whereas, bromo substituted $\mathbf{HL_1}$ selectively detects Zn^{2+} ions due to its intermediate basic character.

View Article Online
DOI: 10.1039/C9DT04902A

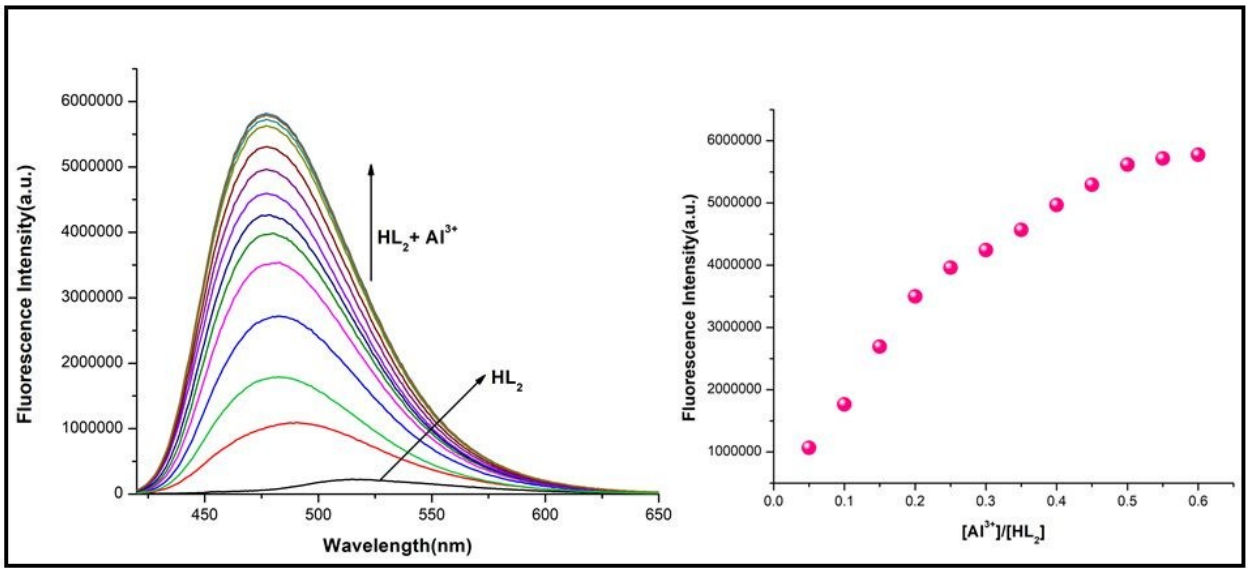

Fig. 6 Fluorescence titration of $\mathbf{HL_2}$ (10 μM) with gradual addition of Al^{3+} (0-6 μM) in 10 mM HEPES buffer at pH 7.4 and corresponding fluorescence intensities versus molar ratio plot.

Selectivity of the probes ($\mathbf{HL_1}$ and $\mathbf{HL_2}$) toward Zn^{2+} and Al^{3+} ions over other competitive species was confirmed by fluorescence titration experiment in presence of different alkali metal ions (Na^+ and K^+), alkaline-earth metal ions (Mg^{2+} and Ca^{2+}), various transition-metal ions (Cr^{3+}, Mn^{2+}, Fe^{3+}, Co^{2+}, Ni^{2+}, Cu^{2+}, Cd^{2+} and Hg^{2+}) and Pb^{2+} ion (Fig. S25 and S26, Supporting Information). Upon addition of different common anions like $S_2O_3^{2-}$, S^{2-}, SO_3^{2-}, HSO_4^-, SO_4^{2-}, SCN^-, N_3^-, OCN^-, AsO_4^-, PO_4^{3-}, ClO_4^-, AcO^-, Cl^-, NO_3^-, $P_2O_7^{4-}$(PPi), PF_6^-, F^- (Fig. S27 and S28, Supporting Information) in HEPES buffer (10 mM) at pH 7.4 to the chemosensors no significant fluorescence enhancement has been noticed. Competition assay experiments also support high fluorescent recognition of $\mathbf{HL_1}$ and $\mathbf{HL_2}$ for Zn^{2+} and Al^{3+} ions over other cations and anions (Fig. 7, S29-S31, Supporting Information). Binding constant values (using equation 1) from fluorescence data ((1.49±0.01) × 10^4 M^{-1} and (1.74±0.01) × 10^4 M^{-1}, for complexes **1** and

View Article Online
DOI: 10.1039/C9DT04902A

2, respectively) are also well matched with the data obtained from UV-Vis study (Fig. S32 and S33, Supporting Information).

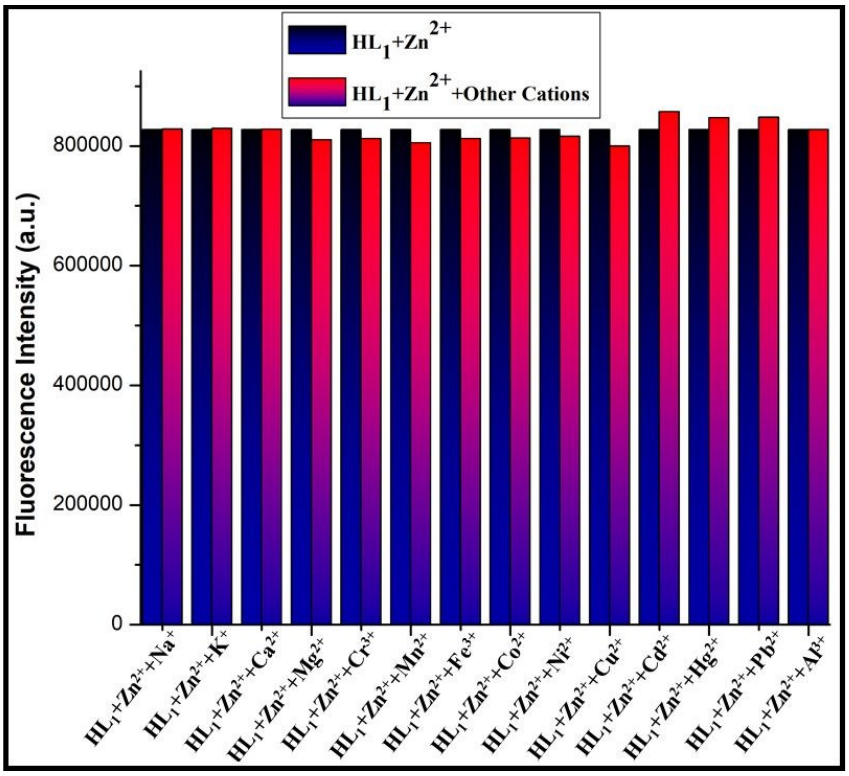

Fig. 7 Relative fluorescence intensity profile of $[(\mathbf{L_1})_2–Zn^{2+}]$ system in the presence of different common cations in 10 mM HEPES buffer at pH 7.4. Here, $\mathbf{HL_1}$= 10 μM; Zn^{2+} = 5 μM; other cations= 50 μM.

Here, fluorescence excitation wavelengths of both the chemosensors are observed in the visible region. Again, they exhibit large Stoke shift in presence of Zn^{2+} and Al^{3+} ions (100 nm and 75 nm, respectively). Visible range excitation wavelengths and large Stoke shift make these systems promising probe in the field of biological study. $\mathbf{HL_1}$ and $\mathbf{HL_2}$ show distinct colour change under UV light in presence of Zn^{2+} and Al^{3+} ions, respectively. $\mathbf{HL_1}$ shows yellow fluorescence in presence of Zn^{2+} ions whereas $\mathbf{HL_2}$ shows sky blue fluorescence in presence of Al^{3+} ions (Fig. 8).

View Article Online
DOI: 10.1039/C9DT04902A

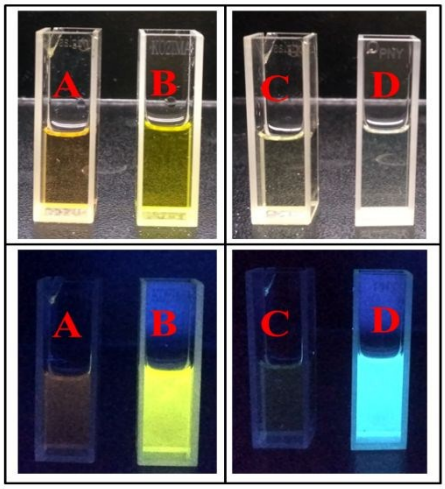

Fig. 8 Visual colour changes of chemo sensors (**HL_1** and **HL_2**) (10μM) in presence of Zn^{2+} and Al^{3+} ions (5 μM) in 10 mM HEPES buffer (pH 7.4) medium. Here, A = **HL_1** (10μM), B = **HL_1** (10μM) +Zn^{2+} (5 μM), C= **HL_2** (10μM) and D = **HL_2** (10μM) +Al^{3+} (5 μM). Above images are taken under normal light and below images are taken under UV lamp.

Reversibility and regeneration experiment is performed in presence of sodium salt of ethylenediaminetetraacetic acid (Na_2EDTA) solution. Yellow colour of **HL_1** - Zn^{2+} solution (1 equivalent) turned pale orange colour with abrupt decrease in fluorescence intensity in presence of Na_2EDTA solution (1 equivalent) and further regeneration of colour and fluorescence intensity in presence of excess Zn^{2+} ions (0.5 equivalent) have been successively observed for five cycles. Similar experiment was performed with **HL_2**, Al^{3+} ions and Na_2EDTA (Fig. S34, Supporting Information). Limit of detection (LOD) of the chemosensors (**HL_1** and **HL_2**) towards Zn^{2+} and Al^{3+} ions are calculated using 3σ method.[55o] The detection limit of the chemosensor for both the ions are 1.39×10^{-7} M and 1.50×10^{-7} M, respectively.

Stability of chemosensors is examined by reversibility experiment[61a] (Fig. S35, Supporting Information). Here, an acidic (pH 4) and a basic pH (pH 10) are chosen. In chemosensors solution, pH values are repeatedly altered for eight cycles by adding 2(M) HCl

View Article Online
DOI: 10.1039/C9DT04902A

and 2(M) NaOH in an alternating fashion. It clearly indicates stability of both chemosensors in a wide range of pH values. The effect of pH on the fluorescence response of the chemosensors (**HL_1** and **HL_2**), towards Zn^{2+} and Al^{3+} ions are examined (Fig. 9 and Fig. S36, Supporting Information). Both free chemosensors **HL_1** and **HL_2** fluoresce weakly over the pH range 3–11. The organic compounds exhibit weak fluorescence due to PET process. A slight fluoresce enhancement at low pH range (3–6) suggest arrest of the PET process due to protonation.[61a] In presence of Zn^{2+} ions a similar pattern in pH 3-6 range suggests no complex formation in acidic condition. An abrupt increase in fluorescence intensity in pH 6-8 suggests deprotonation of ligand followed by formation of $Zn(\mathbf{L_1})_2$ complex. Further increase of pH values from 9-11, fluorescence intensity show no further enhancement. A similar pattern has been found in case of **HL_2** in presence of Al^{3+} ions (Fig. S36, Supporting Information).

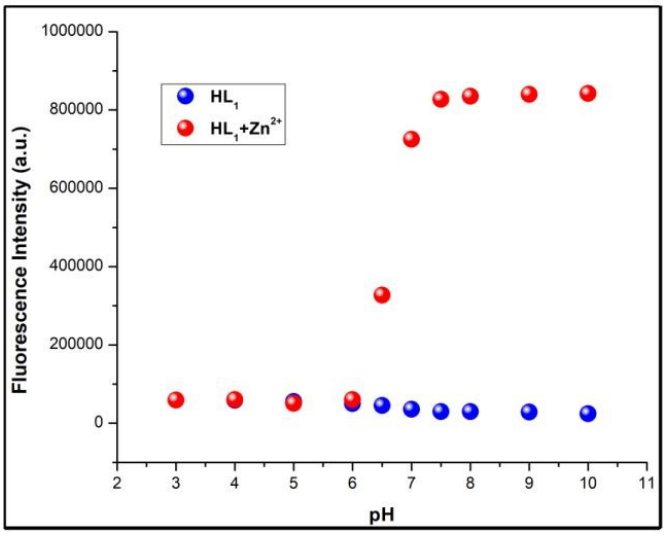

Fig. 9 Fluorescence intensity of **HL_1** (10 μM) in the absence and presence of Zn^{2+}ions (5μM) at various pH values in 10 mM HEPES buffer.

View Article Online
DOI: 10.1039/C9DT04902A

Life time and quantum yield measurements

Lifetime experiment for the chemosensors (**HL_1** and **HL_2**) and complexes **1** and **2** are studied at 298 K in 10 mM HEPES buffer (pH 7.4) medium. The values of fluorescence lifetime of **HL_1**, **HL_2**, complexes **1** and **2** are 3.15, 1.45, 3.91 and 1.50 ns, respectively (Fig. 10).

Fluorescence quantum yield (Φ) has been calculated by the using following formula:

$$\Phi_{sample} = \{(OD_{standard} \times A_{sample} \times \eta^2_{sample})/(OD_{sample} \times A_{standard} \times \eta^2_{standard})\} \times \Phi_{standard}$$

Where, A is the area under the emission spectral curve, OD is the optical density of the compound at the excitation wavelength and η is the refractive index of the solvent. Here the value of $\Phi_{standard}$ is taken as 0.52 (for Quinine Sulfate).

The values of Φ for **HL_1**, **HL_2**, complexes **1** and **2** are found to be 0.019, 0.054, 0.170 and 0.210, respectively (Table S3, Supporting Information).

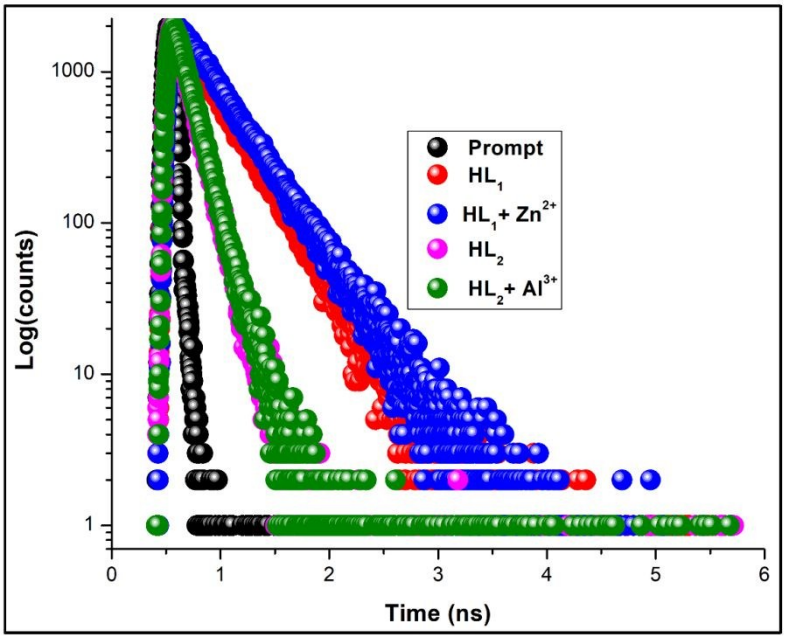

Fig. 10 Time-resolved fluorescence decay curves (logarithm of normalized intensity vs time in ns) of **HL_1**, **HL_2**, complexes **1** and **2**.

View Article Online
DOI: 10.1039/C9DT04902A

Cell imaging study

The fluorescence microscopy study helps to envisage the cellular uptake of 20 μM of probe **HL$_1$** and 10 μM of Zn^{2+} ions as well as in case of **HL$_2$** and Al^{3+} ions. A prominent green and blue fluorescent signal is observed under the microscope after the internalization of chemosensors (**HL$_1$**and **HL$_2$**) and Zn^{2+} and Al^{3+} ions as depicted in Fig. 11. Thus we can conclude that the cells readily internalize the ligands (**HL$_1$** and **HL$_2$**) and the Zn^{2+} and Al^{3+} salt which results in green and blue fluorescent signal, respectively.

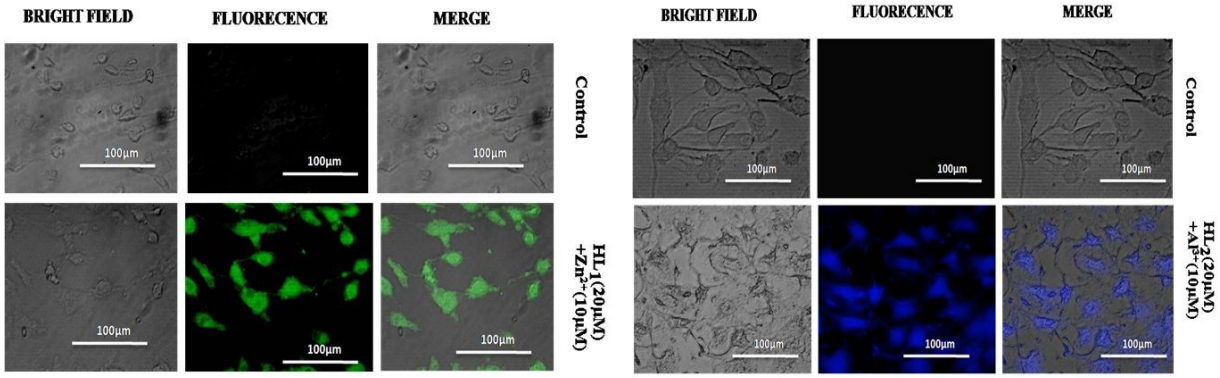

Fig. 11 Bright field, fluorescence and merged microscopic images of untreated *MDA-MB-468* (Control), cells treated with **HL$_1$** (20 μM) + Zn^{2+} (10μM) ions and **HL$_2$** (20 μM) + Al^{3+} (10μM) ions, respectively.

Cell survivability assay

The cellular cytotoxicity of the **HL$_1$** and **HL$_2$** are estimated for checking the biocompatibility on *WI38* cell line. The cells are treated with five different concentrations (0 μM, 20 μM, 40 μM, 60 μM, 80 μM and 100 μM) of chemosensors for 24h and followed by MTT assay. It is observed that the probes (**HL$_1$** and **HL$_2$**) exhibit no significant toxicities even at

View Article Online
DOI: 10.1039/C9DT04902A

the highest concentration of 100 μM (Fig. 12). Therefore these two chemosensors can be considered as biocompatible and they can emerge as potential agents for biomedical applications.

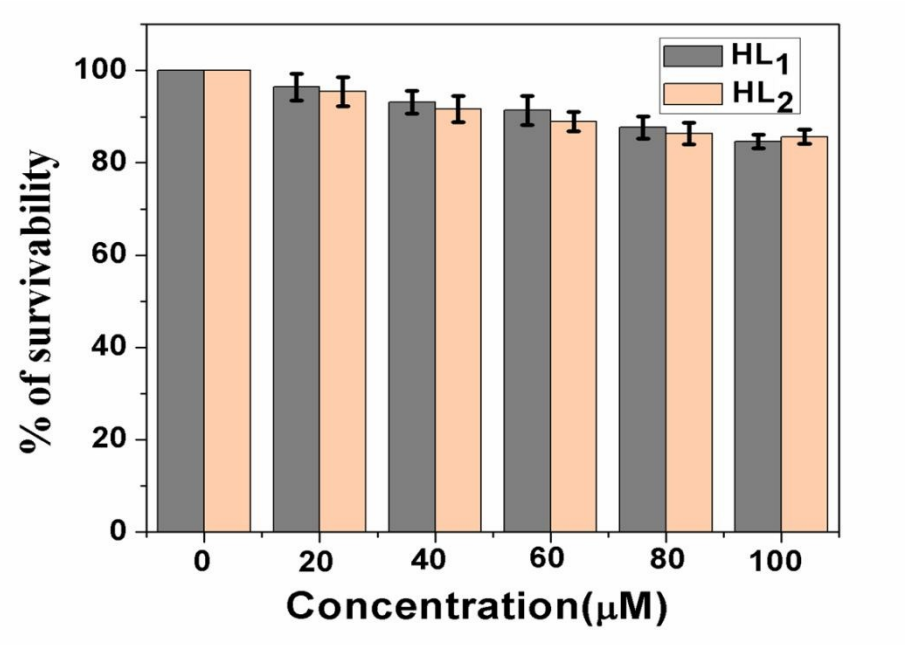

Fig. 12 Cell survivability of *WI38* cells exposed to $\mathbf{HL_1}$ and $\mathbf{HL_2}$.

Anticancer activity of complexes 1 and 2

The cytotoxicity of complex **1** and complex **2** on breast cancer cells, *MDA-MB-468* cells and human cervical cancer cells, *SiHa* is examined by MTT assay to establish their lethal effects towards these cancerous cells. Treatment with different concentrations of both complexes **1** and **2** (1-120 μM) for 24 h, reduce the cell viability significantly in a dose-dependent manner. Complex **1** exhibited lower LD-50 value for both the cell lines (Fig. 13a, b). The LD-50 values of complexes **1** and **2** are given in Table S4 (Supporting Information) and the respective LD-50 values are chosen for the entire experimentation using *MDA-MB 468* cells.

The intracellular reactive oxygen species (ROS) is envisaged with the aid of spectrofluorometry where 2', 7' dichlorofluorscence in diacetate (DCF-DA) is used as a specific

View Article Online
DOI: 10.1039/C9DT04902A

probe. The images reveal that the green color fluorescent intensity is enhanced for both treated cells compared to control cells in *MDA-MB 468* cell lines after 12h (Fig. S37, Supporting Information).

We have further investigated the effects on mitochondrial damage by JC-1 staining which showed a drastic alteration of the redox status of cellular mitochondria in response to complexes **1** and **2** (Fig. 13c). The transition of fluorescence from red to green or a decrease in the red/green ratio indicated the increase in the mitochondrial permeability in response to complexes **1** and **2**.

In order to establish whether complexes initiated in the induction of apoptosis but not necrosis, flow cytometric evaluation is performed employing Annexin-V-FITC/PI staining by envisaging the level of exposed phosphatidylserine in the outer membrane of cells. The results demonstrate that the percentage of apoptotic (early and late) cells are increased after 24 h of treatment of complex **1** and complex **2** (Fig. 13d) in comparison to the untreated cells.

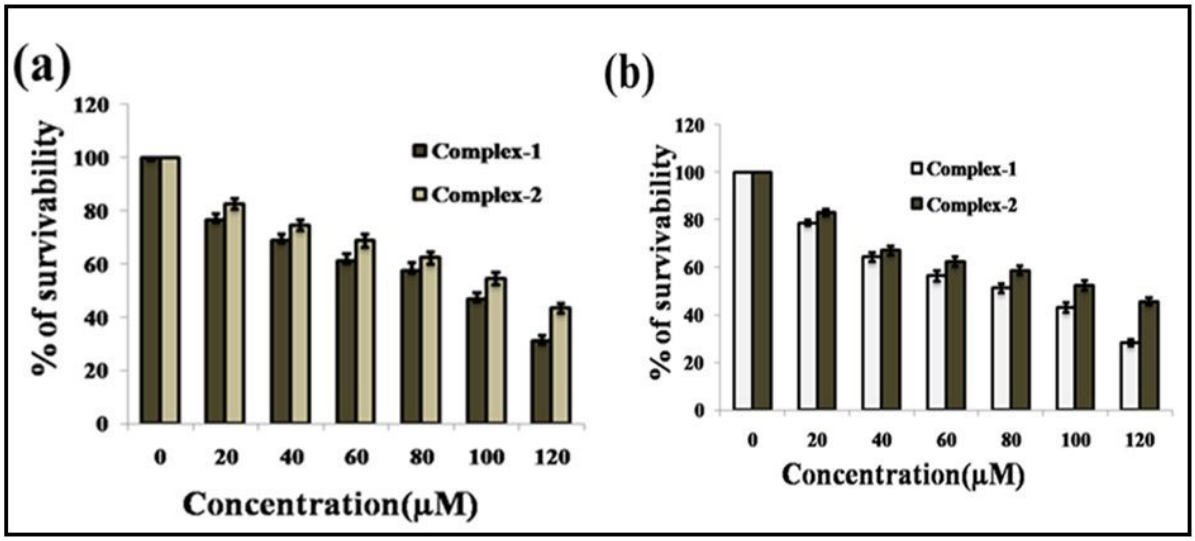

Fig. 13 Effect of increasing doses (0–120 μM) of complexes **1** and **2** on (a) MDA-MB 468 and (b) SiHa cell lines in 24 h.

View Article Online
DOI: 10.1039/C9DT04902A

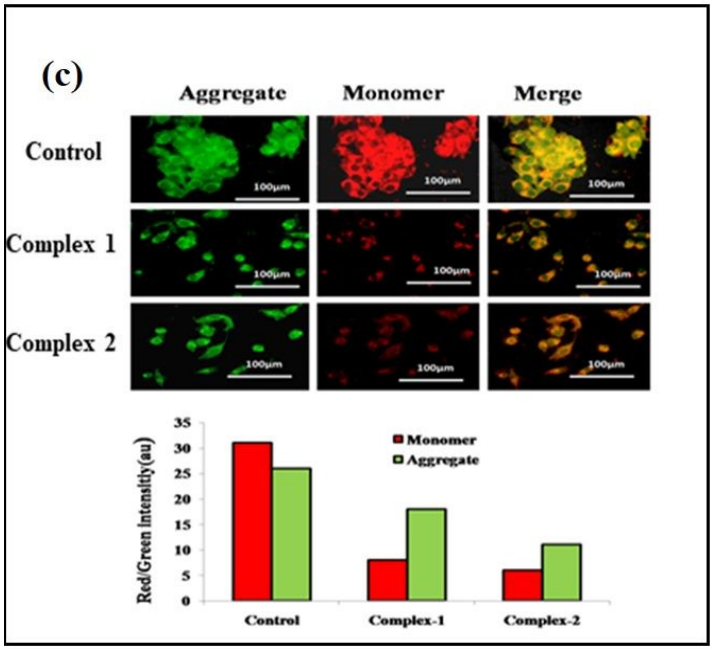

Fig. 13 (c) Mitochondrial membrane potential measurement by JC1 on MDA-MB 468 cells which clearly indicates the mitochondrial membrane potential transition in cells treated with the complexes **1** and **2**.

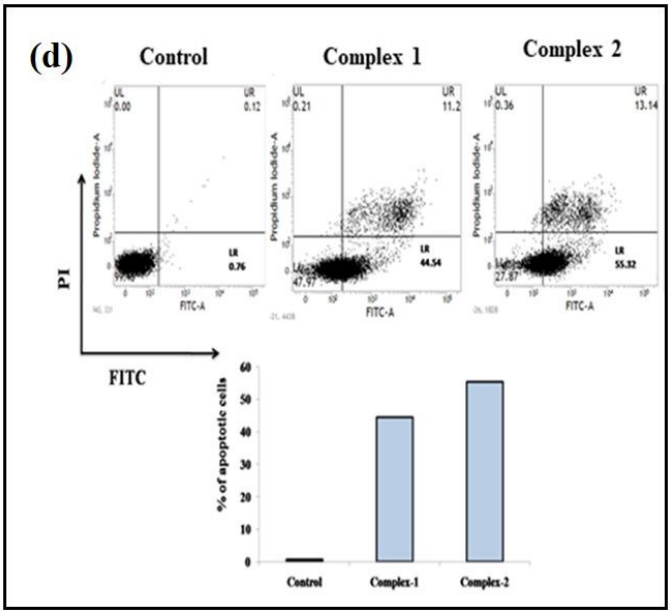

Fig. 13 (d) Comparative study of Annexin V-FITC/PI cells after treatment with LD 50 values of complex **1** and complex **2** by flow cytometry with the control.

View Article Online
DOI: 10.1039/C9DT04902A

Mechanism behind anticancer activity of the complexes 1 and 2

In case of in-vitro study, the complex induce enhancement of intracellular ROS generation has been observed (Fig. S37, Supporting Information). This augmented ROS in turn induces mitochondrial potential dysfunction as we have seen in case of JC-1 study. The mitochondrial membrane disruption is responsible for inducing programmed cell death or apoptosis as illustrated in AnnexinV-FITC studies. The overall anticancer mechanism of our synthesized complexes is depicted schematically in scheme S2 (Supporting Information).

DFT and TDDFT studies

DFT and TDDFT studies are further performed to support structure of the probes. Furthermore, TDDFT studies are performed to understand nature, origin and contribution of M.O.s of electronic transitions. It also gives idea of quantity of energy associated with every individual transition.

Here, geometry optimization of the chemosensors (**HL_1**and **HL_2**) has been performed using DFT/B3LYP method. The optimized structures are depicted in Figs. S38 and S39 (Supporting Information). Energy (eV) of some selected M.O.s are presented in Table S5. Contour plots of some selected molecular orbital of the chemosensors are collected in Fig. S40 (Supporting Information). It has been observed that in both **HL_1** and **HL_2** electron density in LUMO is distributed over the whole molecule and electron density in HOMO is mainly distributed over salicyl and imine part.

Electronic transitions in chemosensors (**HL_1** and **HL_2**) are theoretically studied using TDDFT were B3LYP/CPCM method is used with same basis sets in water. Calculated electronic transitions are given in Table S6. Theoretical calculations show that **HL_1** has intense absorption bands at around 353 and 474 nm for ligand based $\pi\rightarrow\pi^*$ and $n\rightarrow\pi^*$ transition, respectively.

View Article Online
DOI: 10.1039/C9DT04902A

Major transitions for **HL_1** are HOMO-1→LUMO (93%) and HOMO →LUMO (99%) based (Fig. 14) whereas for **HL_2**, the key transitions are HOMO-3→LUMO (48%) and HOMO→LUMO (99%) corresponding to the theoretical absorbance band at 336 and 442 nm, respectively (Fig. S41).

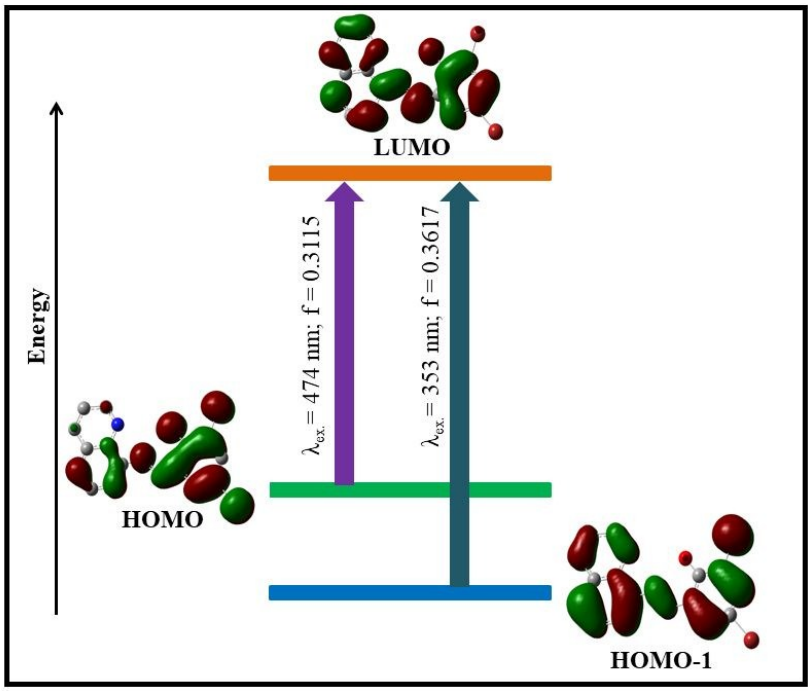

Fig. 14 Pictorial representation of key transitions of chemosensor **HL_1**.

Conclusion

Here we have reported two quinoline based chemosensors (**HL_1** and **HL_2**) for selective detection of Zn^{2+} and Al^{3+} ions. Both the probes exhibit fluorescence excitation in visible region during sensing experiment. Large Stoke shift of the probes in presence of $Zn^{2+}$and Al^{3+} ions suggest their applicability in various fields such as investigation of biological processes, pathological analysis, and therapeutic effects over long time spans. Interestingly, the

View Article Online
DOI: 10.1039/C9DT04902A

chemosensors are achieved by simply changing substituent in the ligand framework. Change of substituent from bromo to nitro, transfer the ligand from soft donor centre to hard donor centre according to HSAB theory. Due to hard basic character of the nitro-substituted chemosensor, it selectively detects Al^{3+} ions. On the contrary, bromo substituted chemosensor selectively detects Zn^{2+} ions due to its comparatively soft rather intermediate basic character. In presence of Zn^{2+} and Al^{3+} ions, chemosensors $\mathbf{HL_1}$ and $\mathbf{HL_2}$ exhibit 30 times and 29 times enhancement of emission intensity. The detection limit (LOD) of $\mathbf{HL_1}$ and $\mathbf{HL_2}$ against Zn^{2+} and Al^{3+} ions are 1.39×10^{-7} M and 1.50×10^{-7} M, respectively which clearly indicate that the probes can be used to detect Zn^{2+} and Al^{3+} ions in biological system. Binding affinity of both metal ions towards the chemosensors (~10^4 orders) and the values of quantum yield of metal bound chemosensors (0.17 and 0.21 for complexes **1** and **2**, respectively) suggest that the probes has significant affinity towards the respective metal ions. X-ray crystal structure of both Al^{3+} and Zn^{2+} ions bound chemosensors prove PET Off-CHEF On mechanism. Importantly, to the best of our knowledge we are first time reported Al^{3+} bound quinoline based chemosensor complex. We have successfully envisaged the practical application of our synthesized chemosensors ($\mathbf{HL_1}$ and $\mathbf{HL_2}$) by performing the bio-imaging experiments in live *MDA-MB-468* cells. Our synthesized probes are able to detect intracellular Zn^{2+} and Al^{3+} ions in cancer cells without exerting any significant cytotoxic effects. Furthermore, the complexes **1** and **2** also exhibit promising anticancer activities through the induction of apoptosis.

Experimental section

Materials and physical measurements

All reagent or analytical grade chemicals and solvents were purchased from commercial sources and used without further purification. Nitrate salts of all cations and sodium salts of all

View Article Online
DOI: 10.1039/C9DT04902A

anions are used for all spectroscopic analysis. Elemental analysis for C, H and N was carried out using a Perkin–Elmer 240C elemental analyzer. Infrared spectra (400-4000 cm^{-1}) were recorded from KBr pellets on a Nicolet Magna IR 750 series-II FTIR spectrophotometer. Absorption spectra were measured using a Cary 60 spectrophotometer (Agilent) with a 1-cm-path-length quartz cell. Electron spray ionization mass (ESI-MS positive) spectra were recorded on a MICROMASS Q-TOF mass spectrometer. Emission spectra were collected using Fluromax-4 spectrofluorimeter at room temperature (298 K) in HEPES buffer at pH= 7.4 solution under degassed condition. Fluorescence lifetime was measured using a time-resolved spectrofluorometer from IBH, UK. Measurements of ^1H NMR spectra were conducted using a Bruker 300 spectrometer instrument in DMSO-d_6 solvent. Thermo gravimetric analysis (TGA) were performed under N_2 atmosphere (150 mL/min) using Platinum crucibles with alpha alumina powder as reference in a PerkinElmer instrument (Model No.- Pyris Diamond TG/DTA).

X-ray crystallography

Single crystal X-ray data of complexes **1** and **2** were collected on a Bruker SMART APEX-II CCD diffractometer using graphite mono chromated Mo Kα radiation (λ = 0.71073 Å) at room temperature. Data processing, structure solution, and refinement were performed using Bruker Apex-II suite program. All available reflections in $2\theta_{max}$ range were harvested and corrected for Lorentz and polarization factors with Bruker SAINT plus.[62] Reflections were then corrected for absorption, inter-frame scaling, and other systematic errors with SADABS.[63] The structures were solved by the direct methods and refined by means of full matrix least-square technique based on F^2 with SHELX-2017/1 software package.[64] All the non hydrogen atoms were refined with anisotropic thermal parameters. C-H hydrogen atoms were inserted at

View Article Online
DOI: 10.1039/C9DT04902A

geometrical positions with U_{iso} = 1/2U_{eq} to those they are attached. Crystal data and details of data collection and refinement for **1** and **2** are summarized in Table S1.

Synthesis of chemosensor (HL_1) [HL_1 = 2,4-Dibromo-6-((quinolin-8-ylimino)methyl)phenol]

Quinoline based Schiff base ligands were prepared by a reported procedure.[61] Briefly, a 1:1 molar ratio mixture of 8-aminoquinoline (2.0 mmol, 0.288 g) and 3,5-dibromosalicylaldehyde (2.0 mmol, 0.558 g) was taken in a R.B. in methanol solvent and stirred for 3h. A deep red coloured solid product was obtained after evaporation of the solvent in good yield and used without further purification.

Yield: 0.357 g (88%). Anal. Calc. for $C_{16}H_{10}Br_2N_2O_3$: C 47.33%; H 2.48%; N 6.90%. Found: C 46.76%; H 2.01%; N 6.07%. IR (cm^{-1}, KBr): υ(C=N) 1609s; υ(C-H) 747s. ESI-MS (positive) in MeCN: The base peak was detected at *m/z* = 406.98, corresponding to $[\mathbf{HL_1}+H]^+$. UV-Vis, λ_{max} (nm), (ε ($dm^3mol^{-1}cm^{-1}$)) in HEPES buffer at pH= 7.4: 340 (79410) and 480 (38171). Melting point ~146 °C.

^{1}H NMR (DMSO-d_6, 300 MHz) δ ppm: 7.69 (Ar-H) (q, 1H), 7.75 (Ar-H) (t, 1H, *J* = 9.00 Hz),7.78 (Ar-H) (d, 1H, *J* = 3.00 Hz), 7.92 (Ar-H) (d, 1H, *J* = 3.00 Hz),7.99 (Ar-H) (s, 1H),8.02 (Ar-H) (s, 1H),8.48 (Ar-H) (d, 1H, *J* = 6.00 Hz), 9.06 (Ar-H) (d, 1H, *J* = 3.00 Hz), 9.27 (-CH=N) (s, 1H), 15.94 (Ar-OH) (s, 1H).

^{13}C NMR (DMSO-d_6, 75 MHz) δ ppm: 106.84, 115.46, 117.87, 119.62, 123.09, 127.28, 127.97, 129.08, 133.64, 135.07, 136.29, 136.91, 139.15, 151.45, 160.72, 163.83.

Synthesis of chemosensor (HL_2) [HL_2= 4-Nitro-2-((quinolin-8-ylimino)methyl)phenol]

The Schiff base ligand $\mathbf{HL_2}$ was also prepared by the above mentioned procedure. Briefly, a 1:1 molar ratio mixture of 8-aminoquinoline (2.0 mmol, 0.288 g) and 2-hydroxy-5-

View Article Online
DOI: 10.1039/C9DT04902A

nitrobenzaldehyde (2.0 mmol, 0.334 g) was taken in a R.B. in methanol solvent and stirred for 3h. An orange coloured solid product was obtained after evaporation of the solvent in good yield and used without further purification.

Yield: 0.255 g (87%). Anal. Calc. for $C_{16}H_{11}N_3O_3$: C 65.53%; H 3.78%; N 14.33%. Found: C 64.86%; H 3.01%; N 13.97%. IR (cm^{-1}, KBr): υ(C=N) 1603s; υ(C-H) 754s. ESI-MS (positive) in MeOH: The base peak was detected at *m/z* = 294.11, corresponding to $[\mathbf{HL_2}+H]^+$. UV-Vis, λ_{max} (nm), (ε ($dm^3mol^{-1}cm^{-1}$)) in HEPES buffer at pH= 7.4: 325 (53837) and 450 (31663). Melting point ~232 °C.

^{1}H NMR (DMSO-d_6, 300 MHz) δ ppm: 6.90 (Ar-H) (d, 1H, *J* = 12.00 Hz), 7.71 (Ar-H) (q, 1H), 7.77 (Ar-H) (t, 1H, J_1 = 9.00 Hz,J_2 = 6.00 Hz),8.04 (Ar-H) (d, 1H, *J* = 6.00 Hz), 8.08 (Ar-H) (d, 1H, *J* = 6.00 Hz), 8.17-8.21 (Ar-H) (m, 1H),8.51 (Ar-H) (d, 1H, *J* = 9.00 Hz),8.67 (Ar-H) (d, 1H, *J* = 3.00 Hz), 9.05 (Ar-H) (d, 1H, *J* = 6.00 Hz), 9.53 (-CH=N) (s, 1H), 16.03 (Ar-OH) (s, 1H).

^{13}C NMR (DMSO-d_6, 75 MHz) δ ppm: 117.94, 121.89, 122.70, 123.20, 124.96, 127.30, 128.03, 128.18, 129.04, 129.84, 131.15, 131.97, 136.29, 136.99, 151.49, 161.62.

Synthesis of {[Zn(L_1)$_2$].$CHCl_3$} (complex 1)

A 2 mL methanolic solution of zinc nitrate hexahydrate (0.50 mmol, 0.149 g) was added drop wise to 20 mL chloroform solution of $\mathbf{HL_1}$ (1.0 mmol, 0.406 g) followed by addition of triethylamine (1.0 mmol, ~0.2 mL) and the resultant reaction mixture was stirred for ca. 3 h. X-ray quality intense brown coloured single crystals were obtained in high yield after slow evaporation of the solvent.

Yield: 0.682 g (78%). Anal. Calc. for $C_{32}H_{18}Br_4N_4O_2Zn$: C 43.90%; H 2.07%; N 6.40%. Found: C 43.01%; H 1.91%; N 5.92%. IR (cm^{-1}, KBr): υ(C=N) 1615s; ν(C-H) 759s. ESI-MS (positive)

View Article Online
DOI: 10.1039/C9DT04902A

in MeCN: The base peak was detected at *m/z* = 923.52, corresponding to $[Zn(\mathbf{L_1})_2+CH_3CN+Li]^+$. UV-Vis, λ_{max} (nm), (ε ($dm^3mol^{-1}cm^{-1}$)) in HEPES buffer at pH= 7.4: 440 (52839). Melting point >250 °C.

^{1}H NMR (DMSO-d_6, 300 MHz) δ ppm: 7.43 (Ar-H) (q, 2H), 7.50 (Ar-H) (d, 2H, *J* = 3.00 Hz),7.73 (Ar-H) (d, 2H, *J* = 3.00 Hz), 7.90 (Ar-H) (d, 2H, *J* = 6.00 Hz),7.99 (Ar-H) (d, 2H, *J* = 9.00 Hz),8.22 (Ar-H) (d, 2H, *J* = 3.00 Hz),8.33 (Ar-H) (d, 2H, *J* = 3.00 Hz), 8.48 (Ar-H) (d, 2H, *J* = 9.00 Hz), 9.34 (-CH=N) (s, 2H).

^{13}C NMR (DMSO-d_6, 75 MHz) δ ppm: 111.71, 113.41, 123.49, 124.26, 124.67, 127.88, 128.46, 128.92, 129.22, 133.68, 138.84, 138.99, 140.99, 151.54, 156.40, 163.71.

Synthesis of {$[Al(L_2)_2](NO_3)$} (complex 2)

A 2 mL methanolic solution of aluminium nitrate nonahydrate (1.0 mmol, 0.187 g) was added drop wise to 20 mL methanolic solution of $\mathbf{HL_2}$ (1.0 mmol, 0.293 g) followed by addition of triethylamine (1.0 mmol, ~0.2 mL) and the resultant reaction mixture was stirred for ca. 1 h. intense green coloured solid mass was obtained after slow evaporation of the solvent.

Yield: 0.759 g (85%). Anal. Calc. for $C_{32}H_{20}N_7O_9Al$: C 57.07%; H 2.99%; N 14.56%. Found: C 56.77%; H 2.47%; N 14.05%. IR (cm^{-1}, KBr): υ(C=N) 1615s; υ(NO_3^-) 1318s; υ(C-H) 771s. ESI-MS (positive) in MeCN: The base peak was detected at *m/z* = 611.29 corresponding to $[Al(\mathbf{L_2})_2]^+$. UV-Vis, λ_{max} (nm), (ε ($dm^3mol^{-1}cm^{-1}$)) in HEPES buffer at pH= 7.4: 398 (19388). Melting point >250 °C.

^{1}H NMR (DMSO-d_6, 300 MHz) δ ppm: 6.61 (Ar-H) (d, 2H, *J* = 9.00 Hz), 7.63 (Ar-H) (q, 2H), 8.12-8.20 (Ar-H) (m, 4H),8.29 (Ar-H) (d, 2H, *J* = 9.00 Hz), 8.68 (Ar-H) (d, 2H, *J* = 3.00 Hz),

View Article Online
DOI: 10.1039/C9DT04902A

8.78 (Ar-H) (d, 2H, J = 6.00 Hz),8.85 (Ar-H) (d, 2H, J = 9.00 Hz),8.96 (Ar-H) (d, 2H, J = 3.00 Hz), 10.27 (-CH=N) (s, 2H).

^{13}C NMR (DMSO-d_6, 75 MHz) δ ppm: 118.41, 119.26, 122.96, 124.40, 129.04, 129.28, 129.65, 132.35, 133.93, 136.76, 136.90, 138.07, 142.00, 148.42, 167.97, 170.41.

UV-visible and fluorescence spectroscopic studies

Stock solutions of various ions (1×10^{-3} M) were prepared in HEPES buffer (pH 7.4) medium. 1×10^{-3} M stock solution of the chemosensors (**HL_1** and **HL_2**) was prepared in methanol. The solutions of **HL_1** and **HL_2** were then diluted to 1×10^{-5} M by HEPES buffer (pH 7.4) as per requirement. Methanol is only used to dissolve the organic chemosensor and the volume of the MeOH solution taken to make the dilution was so small that the MeOH content was deemed to be negligible. All the spectroscopic experiments including competitive assay of various cations and anions were performed in HEPES buffer medium at pH 7.4. In titration experiments, 30 μL solutions of 1×10^{-3} M chemosensors (**HL_1** and **HL_2**) were taken in a quartz optical cell and volume was made up to 3000 μL with buffer, so the solvent again is effectively buffer. In case of **HL_1**, Zn^{2+} solutions were added gradually (0-6 μM) whereas for **HL_2**, Al^{3+} solutions were added gradually to the probe's solution (10μM). In competitive assay experiments, the test samples were prepared in a similar way as mentioned above.

Binding stoichiometry (Job's plot)

Job's continuation method was employed to find out the binding stoichiometry of the chemosensors (**HL_1** and **HL_2**), Zn^{2+} and Al^{3+} ions using absorption spectroscopy. At a given temperature (25ºC), the absorbance was noted for solutions where the concentrations of chemosensors (**HL_1** and **HL_2**), Zn^{2+} and Al^{3+} ions were varied but the sum of their

View Article Online
DOI: 10.1039/C9DT04902A

concentrations was kept constant at 1×10^{-5} M. Change in absorbance was plotted as a function of mole fraction of chemosensor. The break point in the resulting plots corresponds to the mole fraction of chemosensors in Zn^{2+} and Al^{3+} complexes. From the break point, the stoichiometry was estimated. The results reported are average of at least three experiments.

Binding constant calculation

Binding ability of the chemosensors (**HL_1** and **HL_2**) towards Zn^{2+} and Al^{3+} ions were determined using absorption as well as fluorescence spectra. Non-linear least square fitting equation i.e. equation 1 has been employed to determine binding constant value.[55o] OrginPro software, version 8.5 was used to do the necessary fittings and calculations.

$$y = \left(\frac{a + b \times x\text{^}n}{1 + c \times x\text{^}n}\right) \quad \ldots\ldots\ldots\ldots\ldots\ldots\ldots\ldots (1)$$

Where, 'a' and 'b' are the absorbance or fluorescence in absence and presence of excess metal ions, respectively. 'c' is formation constant or binding constant (k) whereas '*n'* is binding stoichiometry of the reaction.

Cell culture

Triple negative human breast cancer cell line *MDA-MB-468*, human cervical cancer cells, *SiHa* and human lung fibroblast cells, *WI38* was obtained from National Center for Cell Science (NCCS) Pune, India. The cells were grown in DMEM with 10% FBS (Fetal Bovine Serum), penicillin/streptomycin (100 units/ml) at 37ºC and 5%CO_2. All the treatments were conducted at 37ºC and at a cell density allowing exponential growth.

Cell imaging

The *MDA-MB-468* cells were grown in coverslips for 24h. Then the cells were either mock-treated or treated with 20µM of ligands (**HL_1** and **HL_2**) and 10µM of Zn^{2+} and Al^{3+},

View Article Online
DOI: 10.1039/C9DT04902A

respectively for 24h at 37ºC. The cells were washed with 1×PBS. Then they were mounted on a glass slide and observed under fluorescence microscope (Leica).

Cell survivability assay

Cell survivability of $\mathbf{HL_1}$ and $\mathbf{HL_2}$ were studied for human lung fibroblast cells, *WI38* (non-cancerous cells), *MDA-MB-468* and *SiHa* (cancerous cells) following reported procedure.[65] In brief, viability of these cells after exposure to various concentrations of ligand were assessed by MTT assay. The cells were seeded in 96-well plates at 1×10^4 cells per well and exposed to ligand at concentrations of 0 μM, 20 μM, 40 μM, 60 μM, 80 μM, 100 μM for 24 h. After incubation, cells were washed with 1×PBS twice and incubated with MTT solution (450μg/ml) for 3-4 h at 37ºC. The resulting formazan crystals were dissolved in an MTT solubilization buffer and the absorbance was measured at 570 nm by using a spectrophotometer (BioTek) and the value was compared with control cells. The cell cytotoxicity of the complex **1** and complex **2** towards the cancer cells *MDA-MB-468* and *SiHa* were also envisaged following the above mentioned MTT assay protocol.

Nuclear morphology study by DAPI staining

Nuclear morphology was studied by DAPI staining. After exposure of complex **1** and complex **2** at their respective LD50 dose for 12h, the cells were washed three times with 1 × PBS and stained with 4′,6-diamidino- 2-phenylindole (DAPI) in Vectashield (0.2 g ml−1, Vector Laboratories Inc.). Nuclear morphology was observed under fluorescence microscope (Leica). A minimum of 400 cells were observed.

View Article Online
DOI: 10.1039/C9DT04902A

Apoptotic and necrotic cell quantification by Annexin V-FITC staining

Apoptotic and necrotic cell was measured by Annexin V-FITC staining. After treatment, cells were washed in ice-cold PBS and incubated with 100 µl of annexin binding buffer. Annexin V-FITC (2 µg/ml) was added and kept in dark at room temperature for 15 min. Then, 400 µl of annexin binding buffer was added. Prior to analysis 5 ml (0.5 mg/ml) PI was added. The estimation of apoptotic and necrotic cells were performed with the help of FACS Calliber.

Method of estimation of reactive oxygen species (ROS)

ROS was estimated by DCF-DA, which enters the cell and reacts with reactive oxygen to give a green fluorescent colour compound dichlorofluorescein (DCF). The estimation of ROS was measured by fluorometer. A stock solution of DCF-DA (10 mM) was prepared in methanol and was further diluted with culture medium to a working concentration of 100 µM. Cells were treated with LD50 doses of complexes for 12 h. Then cells were washed with ice cold Hanks balanced salt solution (HBSS) and incubated with 100 µM (working solution) of DCF-DA for 30 min at 37 °C. Then, cells were lysed with alkaline solutions. Fluorescence intensity was measured at excitation of 485 nm and emission at 520 nm (Biotek).

Computational method

All computations were performed using the GAUSSIAN 09 (G09)[66] software package. For optimization we used the density functional theory method at the B3LYP level[67,68] and the standard 6-31+G(d) basis set for C, H, N and O atoms.[69,70]

TDDFT calculation was performed with the optimized geometry to ensure only positive eigen values. Time-dependent density functional theory (TDDFT)[71–73] was performed using conductor-like polarizable continuum model (CPCM)[74–76] and the same B3LYP level and basis

View Article Online
DOI: 10.1039/C9DT04902A

sets in aqueous solvent system. GAUSSSUM[77] was used to calculate the fractional contributions of various groups to each molecular orbital.

Conflicts of interest

There are no conflicts of interest to declare**.**

Acknowledgments

A. S. gratefully acknowledges the financial support of this work by the DST, India (Sanction No. SB/FT/CS-102/2014, dated- 18.07.2015) and RUSA 2.0, Government of India (Sanction No. R-11/262/19, dated- 08.03. 2019)

Supporting information available

CCDC 1959893 and 1959894 contain the supplementary crystallographic data for complexes **1** and **2**, respectively. These data can be obtained free of charge via http://www.ccdc.cam.ac.uk/conts/retrieving.html, or from the Cambridge Crystallographic Data Centre, 12 Union Road, Cambridge CB2 1EZ, UK; fax: (+44) 1223-336-033; or email:deposit@ccdc.cam.ac.uk.

Notes and references

[a]*Department of Chemistry, Jadavpur University, Kolkata- 700032, India.*

E-mail: amritasahachemju@gmail.com; Tel. +91-33-24572146

[b]*Department of Life Science and Biotechnology, Jadavpur University, Kolkata-700032, India.*

1 (a) R. Ai and Y. He, *Sensors & Actuators: B. Chemical*, 2020*,* **304**, 127372; (b) M. Zhao, J. Wang, H. Yu, Y. He and T. Duan, *Sensors & Actuators: B. Chemical*, 2020, **307**, 127664; (c) M. Zhao, H. Yu and Y. He, *Sensors & Actuators: B. Chemical*, 2019, **283**, 329–333; (d) W. Huang, J. Wang; J. Du1, Y. Deng and Y. He, *Microchimica Acta*, 2019, **186**, 79; (e) Y. Yue and Y. He, *Analytical Sciences*, 2019, **35**, 159–163; (f) M. Li, X. Huang and H. Yu, *Materials Science &*

View Article Online
DOI: 10.1039/C9DT04902A

Engineering C, 2019, **101**, 614–618; (g) Y. He, B. Xu, W. Li, and H. Yu, *J. Agric. Food Chem.*, 2015, **63**, 2930–2934.

2 (a) N. Malviya, C. Sonkar, B. K. Kundu and S. Mukhopadhyay, *Langmuir*, 2018, **34**, 11575–11585; (b) H. Su, S. Zhu, M. Qu, R. Liu, G. Song and H. Zhu, *J. Phys. Chem. C*, 2019, **123**, 15685–15692; (c) J. Liu, Y. –Q. Fan, S. –S. Song, G. –F. Gong, J. Wang, X. –W. Guan, H. Yao, Y. –M. Zhang, T. –B. Wei and Q Lin, *ACS Sustainable Chem. Eng.*, 2019, **7**, 11999−12007; (d) J. Liu, Y. –Q. Fan, Q. –P. Zhang, H. Yao, Y. –M. Zhang, T. –B. Wei and Q. Lin, *Soft Matter,* 2019, **15**, 999−1004; (e) Q. Lin, X. –W. Guan, Y. –M. Zhang, J. Wang, Y. –Q. Fan, H. Yao and T. –B. Wei, *ACS Sustainable Chem. Eng.*, 2019, **7**, 14775−14784; (f) Q. Lin, Y. –Q. Fan, P. –P. Mao, L. Liu, J. Liu, Y. –M. Zhang, H. Yao and T. –B. Wei, *Chem. Eur. J.*, 2018, **24**, 777–783.

3 (a) H. N. Kim, W. X. Ren, J. S. Kim and J. Yoon, *Chem. Soc. Rev.*, 2012, **41**, 3210–3244; (b) L. E. Santos-Figueroa, M. E. Moragues, E. Climent, A. Agostini, R. Martínez-Máñez and F. Sancenón, *Chem. Soc. Rev.*, 2013, **42**, 3489–3613; (c) W. P. Lustig, S. Mukherjee, N. D. Rudd, A. V. Desai, J. Li and S. K. Ghosh, *Chem. Soc. Rev.*, 2017, **46**, 3242–3285; (d) H. Wang, W. P. Lustig and J. Li, *Chem. Soc. Rev.*, 2018, **47**, 4729–4743; (e) X. Wang, T. Qin, S. -S. Bao, Y. -C. Zhang, X. Shen, L. -M. Zheng and D. Zhu, *J. Mater. Chem. A*, 2016, **4**, 16484–16489; (f) S. Yang, W. Jiang, Y. Tang, L. Xu, B. Gao and H. Xu, *RSC Adv.*, 2018, **8**, 37828–37834.

4 M. Li, X. J. Jiang, H. H. Wu, H. L. Lu, H. Y. Li, H. Xu, S. Q. Zang and T. C. W. Mak, *Dalton Trans.*, 2015, **44**, 17326–17334.

5 L. Wang, D. D. Ye, W. X. Li, Y. Y. Liu, L. H. Li, W. L. Zhang and L. Ni, *Spectrochim. Acta A*, 2017, **183**, 291–297.

6 G. Chen, Z. Guo, G. Zeng and L. Tang, *Analyst*, 2015, **140**, 5400–5443.

View Article Online
DOI: 10.1039/C9DT04902A

7 D. T. Quang and J. S. Kim, *Chem. Rev.*, 2010, **110**, 6280–6301.

8 C. F. Mills, *Zinc in Human Biology*; Springer-Verlag: New York, 1989.

9 (a) L. M. T. Canzoniero, S. L. Sensi and D. W. Choi, *Neurobiol. Dis.*, 1997, **4**, 275–279; (b) C. E. Outten and T. V. O'Halloran, *Science*, 2001, **292**, 2488–2492; (c) R. B. Thompson, D. Peterson, W. Mahoney, M. Cramer, B. P. Maliwal, S. W. Suh, C. Frederickson, C. Fierke and P. Herman, *J. Neurosci. Methods*, 2002, **118**, 63–75; (d) L. A. Finney, T. V. O'Halloran, *Science*, 2003, **300**, 931–936.

10 C. J. Frederickson, M. A. Klitenick, W. I. Manton and J. B. Kirkpatrick, *Brain Res.*, 1983, **273**, 335–339.

11 (a) C. J. Frederickson, *Int. Rev. Neurobiol.*, 1989, **31**, 145–238; (b) C. J. Frederickson and A. I. Bush, *Biometals*, 2001, **14**, 353–366; (c) Y. Li, C. Hough and J. Sarvey, *Sci. STKE*, 2003, **182**, 19.

12 (a) P. D. Zalewski, S. H. Millard, I. J. Forbes, O. Kapaniris, A. Slavotinek, W. H. Betts, A. D. Ward, S. F. Lincoln and I. Mahadevan, *J. Histochem. Cytochem.*, 1994, **42**, 877–884; (b) W. J. Qian, K. R. Gee and R. T. Kennedy, *Anal. Chem.*, 2003, **75**, 3468–3475.

13 P. D. Zalewski, X. Jian, L. L. L. Soon, W. G. Breed, R. F. Seamark, S. F. Lincoln, A. D. Ward and F. Z. Sun, *Reprod. Fertil. Dev.*, 1996, **8**, 1097–1105.

14 R. B. Thompson, D. Peterson, W. Mahoney, M. Cramer, B. P. Maliwal, S. W. Suh, C. Frederickson, C. Fierke and P. Herman, *J. Neurosci. Methods*, 2002, **118**, 63–75.

15 E. Mocchegiani, C. Bertoni-Freddari, F. Marcellini and M. Malavolta, *Prog. Neurobiol.*, 2005, **75**, 367–390.

16 J. Hardy and D. J. Selkoe, *Science*, 2002, **297**, 353–356.

17 J. Hardy, *Curr. Alzheimer Res.*, 2006, **3**, 71–73.

View Article Online
DOI: 10.1039/C9DT04902A

18 B. J. Kim, Y. H. Kim, S. Kim, J. W. Kim, J. Y. Koh, S. H. Oh, M. K. Lee, K. W. Kim and M. S. Lee, *Diabetes*, 2000, **49**, 367–372.

19 A. B. Chausmer, *J. Am. Coll. Nutr.*, 1998, **17**, 109–115.

20 (a) E. M. Nolan and S. J. Lippard, *Acc. Chem. Res.*, 2009, **42**, 193–203; (b) E. L. Que, D. W. Domaille and C. J. Chang, *Chem. Rev.*, 2008, **108**, 1517–1549.

21 D. Dambournet, A. Demourgues, C. Martineau, S. Pechev, J. Lhoste, J. Majimel, A. Vimont, J. –C. Lavalley, C. Legein, J. –Y. Buzaré, F. Fayon and A. Tressaud, *Chem. Mater.*, 2008, **20**, 1459–1469.

22 A. Samokhvalov, *Coordination Chemistry Reviews*, 2018, **374**, 236–253.

23 Scientific Opinion of the Panel on Food Additives, Flavourings, Processing Aids and Food Contact Materials (AFC), *The EFSA Journal*, 2008, **754**, 1–34.

24 A. C. Alfrey, G. R. LeGendre and W. D. Kaehny, *New Engl. J. Med.*, 1976, **294**, 184–188.

25 M. K. Ward, T. G. Feest, H. A. Ellis, I. S. Parkinson and D. N. Kerr, *Lancet*, 1978, **1**, 841–845.

26 S. E. Jorgensen and A. Jensen, *Metal Ions Biol. Syst.*, 1984, **18**, 61.

27 S. Jansen, T. Watanabe, E. Smets and S. Jansen, *Annals of Botany*, 2002, **90**, 53–64.

28 A. Frankova, O. Drabek, J. Havlik, J. Szakova and A. Vanek, *J. Inorg. Biochem.*, 2009, **103**, 1480–1485.

29 G. Theriault, C. Tremblay, S. Cordier and S. Cingras, *Lancet*, 1984, **1**, 947–950.

30 A. Ronneberg and F. Langmark, *Am. J. Ind. Med.*, 1992, **22**, 573–590.

31 C. Swain and G. B. N. Chainy, *J. Trace Elem. Med. Biol.*, 1997, **11**, 77–82.

32 C. Cuccarella, C. Montoliu, C. Hermenegildo, R. Saez, L. Manzo, M. D. Minana and V. Felipo, *J. Neurochem.*, 1998, **70**, 1609–1614.

View Article Online
DOI: 10.1039/C9DT04902A

33 Y. Hojo, T. Kobayashi, Y. Shigemitsu and T. Tanabe, *Jpn. J. Toxicol. Environ. Health*, 1998, **44**, P–10.

34. J. A. Edwardson, J. M. Candy, P. G. Ince, F. K. McArthur, C. M. Morris, A. E. Oakley, G. A. Taylor and E. Bjertness, *Ciba Found. Symp.*, 1992, **169**, 165–185.

35 M. Kawahara, *J. Alzheimer Dis.*, 2005, **8**, 171–182.

36 J. Savory, M. M. Herman, C. D. Katsetos and M. R. Wills, in: M. Nicolini, P.F. Zatta, B. Corain (Eds.), Aluminum in Chemistry Biology and Medicine, Cortina International/Raven Press, Verona/New York, 1991, p. 45.

37 C. Exley, G. Mamutse, O. Korchazhkina, E. Pye, S. Srekopytov, A. Polwart and C. Hawkins, *Mult. Scler.*, 2006, **12**, 533–540.

38 Y. Lu, S. Huang, Y. Liu, S. He, L. Zhao and X. Zeng, *Org. Lett.*, 2011, **13**, 5274–5277.

39 (a) Y. Tachapermpon, S. Thavornpradit, A. Charoenpanich, J. Sirirak, K. Burgess and N. Wanichacheva, *Dalton Trans***.**, 2017, **46**, 16251–16256; (b) T. Liu, Y. Dong, X. Wan, W. Li and Y. Yao, *RSC Adv.*, 2015, **5**, 76939–76942.

40 (a) L. Hou, J. Feng, Y. Wang, C. Dong, S. Shuang and Y. Wang, *Sens. Actuators B*, 2017, **247**, 451–460; (b) J. -c. Qin, L. Fan, B. -d. Wang, Z. -y. Yang, T. -r. Li, *Anal.Methods.*, 2015, **7**, 716–722.

41 X. Chen, T. Pradhan, F. Wang, J. S. Kim and J. Yoon, *Chem. Rev.*, 2012, **112**, 1910–1956.

42 H. N. Kim, M. H. Lee, H. J. Kim, J. S. Kim and J. Yoon, *Chem. Soc. Rev.*, 2008, **37**, 1465–1472.

43 V. Dujols, F. Ford and A. W. Czarnik, *J. Am. Chem. Soc.*, 1997, **119**, 7386–7387.

44 D. T. Quang and J. S. Kim, *Chem. Rev.*, 2010, **110***,* 6280–6301.

45 B. A. Wong, S. Friedle and S. J. Lippard, *J. Am. Chem. Soc.*, 2009, **131**, 7142–7152.

View Article Online
DOI: 10.1039/C9DT04902A

46 X. Zhang, D. Hayes, S. J. Smith, S. Friedle and S. J. Lippard, *J. Am. Chem. Soc.*, 2008, **130**, 15788–15789.

47 L. Xue, G. Li, D. Zhu, Q. Liu and H. Jiang, *Inorg. Chem.*, 2012, **51**, 10842–10849.

48 L. Xue, Q. Liu and H. Jiang, *Org. Lett.*, 2009, **11**, 3454–3457.

49 (a) H. Liu, Y. Dong, B. Zhang, F. Liu, C. Tan, Y. Tan and Y. Jiang, *Sens. Actuators B*, 2016, **234**, 616–624; (b) H. M. Park, B. N. Oh, J. H. Kim, W. Qiong, I. H. Hwang, K. Jung, C. Kim and J. Kim, *Tetrahedron Letters*, 2011, **52**, 5581–5584; (c) M. Yan, T. Li and Z. Yang, *Inorg. Chem. Communications*, 2011, **14**, 463–465; (d) S. M. Z. Al-Kindy, Z. Al-Mafrigi, M. S. Shongwe and F. E. O. Suliman, *Luminescence*, 2011, **26**, 462–470; (e) X. Zhou, B. Yu, Y. Guo, X. Tang, H. Zhang and W. Liu, *Inorg. Chem.*, 2010, **49**, 4002–4007.

50 Z. Xu, J. Yoon and D. R. Spring, *Chem. Soc. Rev.*, 2010, **39**, 1996–2006.

51 Y. Fu, C. Fan, G. Liu, S. Cui and S. Pu, *Dyes Pigm.*, 2016, **126**, 121–130.

52 (a) Y. Zhang, X. Guo, W. Si, L. Jia and X. Qian, *Org. Lett.*, 2008, **10**, 473–476; (b) C. He, Z. Lin, Z. He, C. Duan, C. Xu, Z. Wang and C. Yan, *Angew. Chem., Int. Ed.*, 2008, **47**, 877–881.

53 I. Ravikumar and P. Ghosh, *Inorg. Chem.*, 2011, **50**, 4229–4231.

54 D. Maity and T. Govindaraju, *Chem. Commun.*, 2012, **48**, 1039–1041.

55 (a) J. Fu, Y. Chang, B. Li, H. Mei, L. Yang and K. Xu, *Analyst*, 2019, **144**, 5706–5716; (b) A. Hazra, A. Roy, A. Mukherjee, G. P. Maiti and P. Roy, *Dalton Trans.*, 2018, **47**, 13972–13989; (c) M. Sohrabi, M. Amirnasr, S. Meghdadi, M. Lutz, M. B. Torbati and H. Farrokhpour, *New J. Chem.,* 2018, **42**, 12595—12606; (d) Q. –F. Li, J. –T. Wang, S. Wu, G. –W. Ge, J. Huang, Z. Wang, P. Yang and J. Lin, *Sensors and Actuators B*, 2018, **259**, 484–491; (e) K. Boonkitpatarakul, A. Smata, K. Kongnukool, S. Srisurichan, K. Chainok and M. Sukwattanasinitt, *Journal of Luminescence,* 2018, **198**, 59–67; (f) Y. Dong, R. Fan, W. Chen, P.

View Article Online
DOI: 10.1039/C9DT04902A

Wang and Y. Yang, *Dalton Trans.*, 2017, **46**, 6769–6775; (g) K. Du, S. Niu, L. Qiao, Y. Dou, Q. Zhu, X. Chen and P. Zhang, *RSC Adv.*, 2017, **7**, 40615–40620; (h) M. Sohrabi, M. Amirnasr, H. Farrokhpour and S. Meghdadi, *Sensors and Actuators B*, 2017, **250**, 647–658; (i) A. Roy, S. Dey and P. Roy, *Sensors and Actuators B*, 2016, **237**, 628–642; (j) W. –J. Qu, J. Guan, T. –B. Wei, G. –T. Yan, Q. Lin and Y. –M. Zhang, *RSC Adv.*, 2016, **6**, 35804–35808; (k) S. Mukherjee and S. Talukder, *Journal of Luminescence*, 2016, **177**, 40–47; (l) R. Shen, D. Liu, C. Hou, J. Cheng and D. Bai, *Anal. Methods*, 2016, **8**, 83–88; (m) Y. Yue, Q. Dong, Y. Zhang, Y. Sun and Y. Gong, *Anal. Methods*, 2015, **7**, 5661–5666; (n) Y. W. Choi, J. J. Lee and C. Kim, *RSC Adv.*, 2015, **5**, 60796–60803; (o) A. B. Pradhan, S. K. Mandal, S. Banerjee, A. Mukherjee, S. Das, A. R. K. Bukhsh and A. Saha, *Polyhedron*, 2015, **94**, 75–82; (p) D. Sarkar, A. Pramanik, S. Jana, P. Karmakar and T. K. Mondal, *Sensors and Actuators B*, 2015, **209**, 138–146; (q) S. Erdemir, O. Kocyigit and S. Malkondu, *J Fluoresc*, 2015, **25**, 719–727.

56 (a) S. K. Sahoo, G. D. Kim and H. J. Choi, *J. Photochem. Photobiol. C*, 2016, **27**, 30–53; (b) S. K. Sahoo, D. Sharma, R. K. Bera, G. Crisponi and J. F. Callan, *Chem. Soc. Rev.*, 2012, **41**, 7195–7227.

57 (a) Y. Dong, R. Fan, W. Chen, P. Wang and Y. Yang, *Dalton Trans.*, 2017, **46**, 6769–6775; (b) S. Goswami, A. Manna, S. Paul, K. Aich, A. K. Das and S. Chakraborty, *Dalton Trans.*, 2013, **42**, 8078–8085.

58 K. P. Carter, A. M. Young and A. E. Palmer, *Chem. Rev.*, 2014, **114**, 4564–4601.

59 W. N. Lipscomb and N. Straeter, *Chem. Rev.*, 1996, **96**, 2375–2434.

60 A. K. Bhanja, C. Patra, S. Mondal, D. Ojha, D. Chattopadhyay and C. Sinha, *RSC Adv.*, 2015, **5**, 48997–49005.

View Article Online
DOI: 10.1039/C9DT04902A

61 (a) J. Mandal, P. Ghorai, P. Brandao, K. Pal, P. Karmakar and A. Saha, *New J. Chem.*, 2018, **42**, 19818–19826; (b) P. Ghorai, A. Dey, A. Hazra, B. Dutta, P. Brandão, P. P. Ray, P. Banerjee and A. Saha, *Cryst. Growth Des.*, 2019, **19**, 6431−6447.

62 G. M. Sheldrick, SAINT, Version 6.02, SADABS, Version 2.03, Bruker AXS Inc., Madison, Wisconsin, 2002.

63 G. M. Sheldrick, SADABS: Software for Empirical Absorption Correction, University of Gottingen, Institute fur Anorganische Chemieder Universitat, Gottingen, Germany, 1999–2003.

64 G. M. Sheldrick, *ActaCryst*., 2015, **C71**, 3–8.

65 (a) A. Pramanik, D. Laha, S. Chattopadhyay, S. K. Dash, S. Roy, P. Pramanik and P. Karmakar, *Materials Science and Engineering C*, **2016**, 65, 327–337; (b) D. Laha, A. Pramanik, S. Chattopadhyay, S. K. Dash, S. Roy, P. Pramanik and P. Karmakar, *RSC Adv.*, 2015, **5**, 68169–68178.

66 M. J. Frisch, G. W. Trucks, H. B. Schlegel, G. E. Scuseria, M. A. Robb, J. R. Cheeseman, G. Scalmani, V. Barone, B. Mennucci, G. A. Petersson, H. Nakatsuji, M. Caricato, X. Li, H. P. Hratchian, A. F. Izmaylov, J. Bloino, G. Zheng, J. L. Sonnenberg, M. Hada, M. Ehara, K. Toyota, R. Fukuda, J. Hasegawa, M. Ishida, T. Nakajima, Y. Honda, O. Kitao, H. Nakai, T. Vreven, J. A. Montgomery Jr., J. E. Peralta, F. Ogliaro, M. Bearpark, J. J. Heyd, E. Brothers, K. N. Kudin, V. N. Staroverov, R. Kobayashi, J. Normand, K. Raghavachari, A. Rendell, J. C. Burant, S. S. Iyengar, J. Tomasi, M. Cossi, N. Rega, J. M. Millam, M. Klene, J. E. Knox, J. B. Cross, V. Bakken, C. Adamo, J. Jaramillo, R. Gomperts, R. E. Stratmann, O. Yazyev, A. J. Austin, R. Cammi, C. Pomelli, J. W. Ochterski, R. L. Martin, K. Morokuma, V. G. Zakrzewski, G. A. Voth, P. Salvador, J. J. Dannenberg, S. Dapprich, A. D. Daniels, O. Farkas, J. B.

View Article Online
DOI: 10.1039/C9DT04902A

Foresman, J. V. Ortiz, J. Cioslowski and D. J. Fox, GAUSSIAN09, Revision D.01, Gaussian Inc., Wallingford, CT, 2009.

67 A. D. Becke, *J. Chem. Phys.*, 1993, **98**, 5648–5652.

68 C. Lee, W. Yang and R. G. Parr, *Phys. Rev. B*, 1988, **37**, 785–789.

69 P. J. Hay and W. R. Wadt, *J. Chem. Phys.*, 1985, **82**, 270–283.

70 W. R. Wadt and P. J. Hay, *J. Chem. Phys.*, 1985, **82**, 284–298.

71 R. Bauernschmitt and R. Ahlrichs, *Chem. Phys. Lett.*, 1996, **256**, 454–464.

72 R. E. Stratmann, G. E. Scuseria and M. J. Frisch, *J. Chem. Phys.*, 1998, **109**, 8218–8224.

73 M. E. Casida, C. Jamorski, K. C. Casida and D. R. Salahub, *J. Chem. Phys.*, 1998, **108***,* 4439–4449.

74 V. Barone and M. Cossi, *J. Phys. Chem. A*, 1998, **102**, 1995–2001.

75 M. Cossi and V. Barone, *J. Chem. Phys*., 2001, **115**, 4708–4717.

76 M. Cossi, N. Rega, G. Scalmani and V. Barone, *J. Comput. Chem.*, 2003, **24**, 669–681.

77 N. M. O'Boyle, A. L. Tenderholt and K. M. Langner, *J. Comput. Chem.*, 2008, **29**, 839–845.

View Article Online
DOI: 10.1039/C9DT04902A

For Table of Contents Use Only

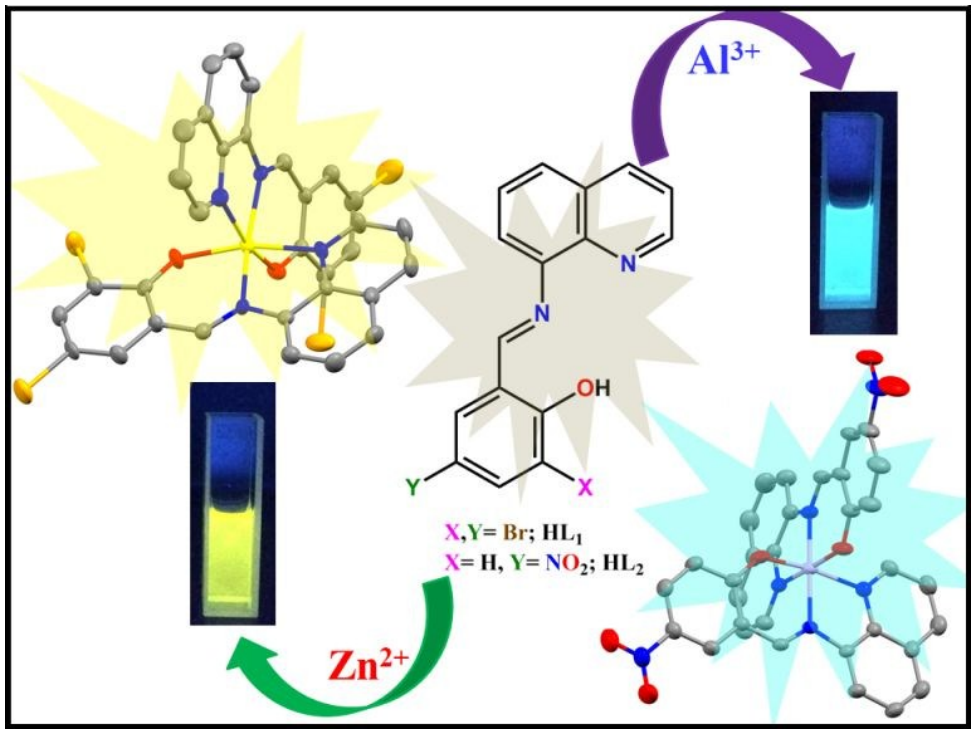

Here, we have reported two aminoquinoline based chemosensors (**HL_1** and **HL_2**) that selectively sense Zn^{2+} and Al^{3+} ions. The sensing phenomena are established by different spectroscopic techniques. We are successful to elucidate the crystal structure of both metal bound chemosensor complexes. Cell imaging study and anticancer activity of the probes and complexes are also investigated.